UNCLASSIFIED Copy No. 6

CONFIDENTIAL

RM No. A7J05

NACA RM No. A7J05

28 JAN 1948

NACA

RESEARCH MEMORANDUM

WIND-TUNNEL INVESTIGATION AT A MACH NUMBER OF 1.53 OF AN AIRPLANE WITH A TRIANGULAR WING

By

Richard Scherrer and William R. Wimbrow

Ames Aeronautical Laboratory
Moffett Field, Calif.

CLASSIFICATION CANCELLED

Authority NACA RA 2356 Date 8/18/54

By [illegible] 8/31/54 See

CLASSIFIED DOCUMENT

This document contains classified information affecting the National Defense of the United States within the meaning of the Espionage Act, USC 50:31 and 32. Its transmission or the revelation of its contents in any manner to an unauthorized person is prohibited by law. Information so classified may be imparted only to persons in the military and naval services of the United States, appropriate civilian officers and employees of the Federal Government who have a legitimate interest therein, and to United States citizens of known loyalty and discretion who of necessity must be informed thereof.

NATIONAL ADVISORY COMMITTEE FOR AERONAUTICS

WASHINGTON

January 23, 1948

NACA LIBRARY
LANGLEY MEMORIAL AERONAUTICAL LABORATORY
Langley Field, Va.

CONFIDENTIAL

UNCLASSIFIED

NASA Technical Library
3 1176 01434 4411

UNCLASSIFIED

NATIONAL ADVISORY COMMITTEE FOR AERONAUTICS

RESEARCH MEMORANDUM

WIND-TUNNEL INVESTIGATION AT A MACH NUMBER OF 1.53 OF AN AIRPLANE WITH A TRIANGULAR WING

By Richard Scherrer and William R. Wimbrow

SUMMARY

An experimental investigation was conducted to determine the aerodynamic characteristics of models of a tailless, pursuit-type, supersonic airplane employing a wing of triangular plan form. Several modifications of the basic airplane were tested and data were obtained at two Reynolds numbers at a Mach number of 1.53. Measurements of lift, drag, and pitching moment were made through an angle-of-attack range of -5° to $+15^{\circ}$, and measurements of side force, drag, and yawing moment were made through an angle-of-yaw range of -1° to $+9^{\circ}$. The wings were equipped with constant-chord, trailing-edge elevators; and the vertical fins with constant-chord, trailing-edge rudders. The elevator deflection angle was varied from 0° to -17.8°. Each of two vertical-tail configurations were tested with rudder angles of 0° and -9°.

The elevator effectiveness was found to be independent of angle of attack through the range investigated and was found to vary linearly with elevator deflection up to a critical deflection angle which could be predicted. It was also found that the effectiveness of the elevators improved with increasing Reynolds number. The models exhibited a variation of drag with lift which was only slightly greater than that predicted by theory.

All of the models tested were longitudinally stable with the center of gravity located at 25 percent of the mean aerodynamic chord. However, with the center of gravity in this position, all the configurations were either directionally unstable or exhibited a degree of stability that appears to be marginal.

INTRODUCTION

A wing of triangular plan form with its apex forward appears to be suitable for certain types of supersonic aircraft because theory indicates that such a wing should have satisfactory subsonic and supersonic stability characteristics and low supersonic wave drag. (See references 1 and 2.) Recently the NACA has completed an experimental investigation

[redacted]

UNCLASSIFIED

of wings of this type. (See reference 3.) Although theory and experiment indicate satisfactory characteristics for wings of triangular plan form, the effect of adding a fuselage and controls to this type of wing requires further investigation. Several types of trailing-edge flaps on triangular wings have been tested in the transonic range and the results of this investigation are reported in reference 4. However, the knowledge of control characteristics of such wings at supersonic speeds is still very limited.

The present investigation was undertaken to determine the aerodynamic characteristics at a Mach number of 1.53 of several configurations for a tailless, pursuit-type, supersonic airplane employing a wing of triangular plan form, and also to determine the control characteristics of constant chord elevators at the trailing edge of such a wing.

SYMBOLS

The following symbols and aerodynamic coefficients (referred to the wind axis) have been used herein:

C_D	drag coefficient $\left(\frac{\text{drag}}{qS}\right)$
C_L	lift coefficient $\left(\frac{\text{lift}}{qS}\right)$
$(\Delta C_L)_e$	change in C_L due to elevator deflection
C_m	pitching-moment coefficient $\left(\frac{\text{pitching moment}}{\bar{c}qS}\right)$
$C_{m_{\frac{\bar{c}}{2}}}$	pitching-moment coefficient referred to the 50-percent M.A.C. station
$\left(\Delta C_{m_{\frac{\bar{c}}{2}}}\right)_e$	change in $C_{m_{\frac{\bar{c}}{2}}}$ due to elevator deflection
$C_{m_{\frac{\bar{c}}{4}}}$	pitching-moment coefficient referred to the 25-percent M.A.C. station
$C_{n_{\frac{\bar{c}}{2}}}$	yawing-moment coefficient referred to the 50-percent M.A.C. station
$C_{n_{\frac{\bar{c}}{4}}}$	yawing-moment coefficient referred to the 25-percent M.A.C. station
C_Y	side-force coefficient $\left(\frac{\text{side force}}{qS}\right)$
M.A.C.	mean aerodynamic chord, $\bar{c}$, inches
q	dynamic pressure, pounds per square foot

M	Mach number
S	total wing area, square inches
S_e	exposed plan area of elevators, square inches
α	angle of attack, degrees
α_δ	rate of change of angle of attack with elevator deflection at a constant lift coefficient
δ_e	elevator deflection angle, degrees
δ_r	rudder deflection angle, degrees
ψ	angle of yaw, degrees

Configuration Symbols

B_s	body with sharp-nose duct entrance
B_{12}	body with open duct entrance and 12° exterior nose angle
K	pilot's canopy
V_1	single vertical fin and rudder
V_2	twin vertical fin and rudders at the wing tips
W_{60}	basic triangular wing with 60° leading-edge sweepback
$W_{60}F$	modified triangular wing with leading-edge fillets

APPARATUS

Wind Tunnel and Balance Equipment

The investigation was conducted in the Ames 1- by 3-foot supersonic wind tunnel No. 1. This wind tunnel is temporarily equipped with a fixed nozzle designed for a Mach number of 1.5 with a 1- by $2\frac{1}{2}$-foot test section. The tunnel, balance, and other instrumentation are described in detail in reference 5. However, in the present investigation, pitching moments were determined by measuring the bending moments in the sting support with a strain gage instead of measuring the reactions on the main balance springs as described in reference 5. This change

introduced a considerable improvement in the accuracy of the moment measurements.

Models

The airplane model tested is an example of a pursuit-type aircraft intended for flight at supersonic speeds. Three-view drawings of the various configurations tested are shown in figure 1 and photographs of the models are shown in figures 2 through 5. The airplane has no horizontal tail and has a fuselage which is large relative to the wing. This size relationship is dictated by the large volume-weight ratio of the ram-jet engine that is to be installed.

The basic wing is an equilateral triangle in plan form and has no dihedral. An NACA 65_1-006.5 airfoil section is used at all spanwise stations. A modified triangular wing with leading-edge root fillets (fig. 5) was also tested. Control surfaces of constant chord (fig. 1) that extend across the entire trailing edge of the wing are to provide longitudinal and lateral control. The elevator deflections were obtained by making a series of similar wings and bending the appropriate portion of the trailing edge of each to the desired angle.

Two vertical fin-rudder configurations are proposed to provide directional stability and control. One configuration (fig. 2) has a large triangular fin with a constant chord rudder and a small ventral fin. Like the wings, the angle of sweepback of the fin leading edge is 60°. The other configuration has twin wing-tip fins, also with constant chord rudders as shown in figure 3. They too are modified equilateral triangles, the lower corner having been cut off to provide ground clearance.

Two body configurations were tested. One incorporated a shock diffuser having a 50° cone at the duct entrance, as shown in figures 2 and 3. The angle of the duct lip was also 50° and the minimum cross-sectional area of the duct occurred at the entrance. The second body had an open-duct divergent entry, the exterior of which was formed by fairing a truncated 12° cone into the cylinderical fuselage as shown in figures 4 and 5. The minimum duct area of this configuration also occurred at the entrance, but unlike the previous configuration no supersonic compression was employed. The latter body was tested both with and without a pilot's canopy. (See fig. 4.)

The models were assembled from interchangeable components that attached to an inner body which was drilled to fit over the end of the sting support and thereby provided a means of attaching the model to the balance beam. The sting was shielded from aerodynamic forces by a shroud that extended to within one-sixteenth inch of the base of the

inner body. This gap allowed the necessary longitudinal motion resulting from the deflection of the drag gages. An orifice was provided in the sting adjacent to the base of the inner body to measure the pressure acting on the base.

METHODS

Test Methods

In the first phase of the tests, aerodynamic forces and moments in pitch were determined through an angle-of-attack range of -5° to $+5^{\circ}$, the normal deflection range of the balance beam. In the next phase, the angle-of-attack range was extended from 5° to 15° by replacing the straight sting support with a sting having a 10° initial angle. Photographs of models installed for both of these phases appear in figure 6. In each test lift, drag, and pitching moments were measured in 1° angle-of-attack increments. As a result of the deflection of the balance beam and the sting, the low angle-of-attack range of the model was slightly greater than the range of the beam. At the high positive angles of attack, the forces acting on the model were great enough to deflect the sting until it fouled against the surrounding shroud. This prevented angles beyond 10° or 12° from being attained at the high dynamic pressure corresponding to the larger Reynolds number.

In the third phase of the test program the various configurations were tested through an angle-of-yaw range of -1° to $+9^{\circ}$. This was accomplished by mounting the models in the tunnel with the span of the wings in a vertical plane as shown in figure 6(c) and by using a sting with a 4° initial angle. Side-force, drag, and yawing moment were measured at 1° increments of angle of yaw.

In all three phases, the angle of attack (or angle of yaw) of the model under load was measured with a vertical cathetometer and, as a check, was also calculated from the measured lift (or side force) and a predetermined spring constant for the balance beam and sting. Both of these methods are described in reference 3.

All models were tested at two Reynolds numbers, 0.71×10^{6} and 1.13×10^{6}, based on the mean aerodynamic chord of the wing. The Reynolds number variation was obtained by varying the total pressure in the wind tunnel.

Method of Analysis

All measured forces were reduced to standard dimensionless coefficients and, to facilitate comparisons, coefficients for all

configurations were based on the dimensions of configuration $B_s W_{50} V_1$. These dimensions are given in table I.

All drag data have been corrected for the effect of the pressure acting on the base of the inner body.

In order to reproduce as closely as possible the flow conditions that would exist over the exterior of the full-scale airplane, it was necessary to provide for air flow through the internal duct of the model. It was considered impractical, however, to design the interior of the model to correspond exactly to the interior of the actual airplane. Therefore, to apply the results obtained from the model tests to actual flight conditions it is necessary to subtract the increment of drag caused by the internal flow in the model from the total measured drag and replace it with a value corresponding to the internal drag of the actual airplane. An approximate value for the internal drag of the models utilizing the B_s duct entrance was obtained in the following manner: First the drag of the B_s fuselage without wings or vertical fins was determined experimentally. Then the 50° entrance cone of the B_s entrance was replaced by another cone that completely plugged the duct entrance. This eliminated the internal flow and consequently the internal drag. To reproduce the original drag or pressure distribution over the exterior of the fuselage aft of the cowling lip, two conditions had to be met: first, the stream angle at the lip had to be the same as with the normal entrance, and second, the pressure at the lip had to be the same. According to calculations the first condition required a 39° cone to block the passage and the second a 48° cone. Since both conditions could not be fulfilled simultaneously, the fuselage was tested with both cones. The pressure drags for the 39°, 48°, and 50° nose cones were calculated by the method of Taylor and Maccoll. (See reference 6.) The internal drag was then assumed to be given by the following equation:

$$D_{internal} = D_{B_s} - \frac{(D_{B_{39}} - D_{39} - D_{39b}) + (D_{B_{48}} - D_{48} - D_{48b})}{2} - D_{50}$$

where

D_{B_s} measured drag of B_s fuselage with normal 50° cone

$D_{B_{39}}$ measured drag of fuselage with 39° cone

$D_{B_{48}}$ measured drag of fuselage with 48° cone

D_{39} calculated drag of 39° cone

D_{48} calculated drag of 48° cone

D_{50} calculated drag of 50° cone

[redacted]

D_{39_b} measured base drag of fuselage with 39° cone

D_{48_b} measured base drag of fuselage with 48° cone

Precision of Results

The accuracy of the experimental data can be determined by estimating the uncertainty of the individual measurements which enter into the determination of the final results. The over-all uncertainty of any given parameter can then be obtained by geometric summation of the uncertainty of each of the factors entering the final value of that parameter. This method of accuracy analysis, described in detail in reference 3, has been applied to the determination of the aerodynamic coefficients for this investigation. Since the accuracy of the results varies nonuniformly with the magnitude of the forces involved (as described in reference 3), an analysis was made for the arbitrary values of 0.2 lift coefficient, 0.06 drag coefficients, and 0.01 moment coefficient. These coefficients are intermediate values obtained for the $B_s W_{60} V_1$ configuration with no elevator deflection. The following values for the uncertainty of the lift, drag, and moment coefficients were obtained:

$$C_L \text{ and } C_Y \pm 0.003$$

$$C_D \pm 0.001$$

$$C_{m_{\frac{\bar{c}}{2}}} \text{ and } C_{m_{\frac{\bar{c}}{4}}} \pm 0.004$$

The major factor contributing to the uncertainty in the moment coefficient was the difficulty in accurately determining the distance between the effective center of the sting moment gage and the centroid of the wing. An error in the measurement of this distance introduces an error in the measured moment coefficient that is constant for that particular model installation. Consequently the slopes of the moment curves can be determined much more accurately than can the actual numerical values of the coefficient. This is demonstrated by the abrupt discontinuities that occur in the moment curves at the point where the change is made from the data obtained with the low angle of attack, straight sting, to that obtained with the high angle, bent sting.

As in reference 3, the uncertainty of the angle-of-attack measurement is ±0.15° and the Mach number may vary by ±0.01.

The average Reynolds numbers for the investigation are 1,130,000 and 710,000, but due to variations in tunnel pressure and temperature the actual value may vary from one test run to another by ±20,000.

The determination of the actual deflection angles of the control surfaces was made extremely difficult by the small size of the models and the fact that these surfaces were bent rather than machined to the desired angle. As a result there was a bend radius rather than a definite hinge line. However, the elevator deflections were measured carefully at six uniformily spaced stations across the span of each wing and the average of these six measurements is used in presenting the data. It is believed that the individual measurements were accurate to $\pm 0.05^{\circ}$ but the values for the various stations across the span of a given wing varied by as much as $\pm 2^{\circ}$ from the average values.

The rudder-deflection angles were subject to variations similar to those of the elevators and, in addition, the chords of the rudders were not constant throughout their length. Consequently no attempt was made to measure the rudder-deflection angles with a high degree of accuracy and the nominal value of -9° for the effective deflection angle of both rudder configurations is subject to an uncertainty of at least $\pm 1^{\circ}$.

RESULTS AND DISCUSSION

Tests in Pitch, Controls Neutral

The variations of lift, drag, and pitching moment with angle of attack were determined for all configurations (table II) through an angle-of-attack range of -5° to $+15^{\circ}$. In this portion of the investigation all the configurations were tested with neutral elevators and rudders.

The internal drag coefficient for the B_s configurations was determined at zero angle of attack by the previously discussed method and is plotted in the appropriate figures. The internal drag correction is assumed to be constant for angles of attack up to 5°.

Configurations B_s and $B_s W_{so}$.- The data presented in figure 7 indicate that the body represents the major portion of the drag of the particular configuration. The lift-curve slope $\left(\frac{dC_L}{d\alpha} = 0.045\right)$ of the $B_s W_{so}$ configuration is in general agreement with that obtained for a similar plan-form wing in the investigation reported in reference 3. The pitching-moment coefficient exhibits a definite nonlinear variation with changing angle of attack. As a result the neutral point varied with angle of attack. Because of this effect, the moment data are shown for two center-of-gravity positions (25 percent and 50 percent M.A.C.) rather than moment curve slope as a function of

center-of-gravity position. The wing-body combination is slightly unstable at zero lift with the center of gravity at the 50-percent M.A.C. position.

A comparison of the curves of figure 8 indicates that the measured drag is only slightly greater than would be predicted by the linear theory, considering leading-edge suction. This result is not in agreement with the data presented in reference 3 for a wing of similar plan form but with an isosceles triangle for the airfoil section. Part of the apparent leading-edge suction effect shown in figure 8 is undoubtedly due to the use of subsonic airfoil section. However, it is possible that there is a favorable interaction between the wing and body pressure fields because of the size of the body in relation to the wing. This latter possibility is indicated by the small drag increment at zero lift between the drag of the B_s and B_s W_{60} configurations. (See fig. 7.) The results of the present investigation indicate either leading-edge suction or wing-body interaction effects but do not indicate which effect predominates or why. Further research is necessary to provide an answer to this question.

Configurations B_s W_{60} V_1 and B_{12} W_{60} V_1.- A comparison of the data in figures 9 and 10 reveals that the configuration utilizing the B_{12} body has approximately 20 percent less measured minimum drag than the otherwise similar configuration with the B_s body. Although the internal drag of the B_{12} body may be lower than that of the B_s body, this could not be expected to account for the entire difference in total drag because the internal drag of the B_s body is about 25 percent of the total drag of the complete configuration. The duct-entrance areas for the B_s and B_{12} configurations were almost identical but the entrance conditions were sufficiently different so that the internal air-flow rate for the B_s body was of the order of 25 percent greater than that of the B_{12} body. Although this might indicate a greater internal drag for the B_s configuration, the unknown differences in internal pressure due to the duct shapes and internal friction make any general conclusions impossible.

The schlieren photographs of the two configurations (figs. 11 and 12) offer a possible explanation for the higher drag of the B_s configurations. Figure 11 shows that the bow shock wave of the B_{12} W_{60} V_1 configuration is attached to the entrance lip and is completely swallowed by the duct. Figure 12 shows that a normal shock wave stands off the lip of the B_s entrance. An entrance of this type is most efficient when the shock wave originating at the nose of the entrance cone intersects the lip of the entrance, when the lip angle of the entrance is identical with the local stream angle, and when the lip tapers to zero thickness. None of these conditions were met

in the model tested and consequently, as is shown, the normal shock wave was slightly detached from the duct lip.

The lift-curve slope of the wing-body combination (B_s W_{60}) was unchanged by the addition of the V_1 vertical tail, and the minimum drag coefficient was increased by only 2 percent. The pitching-moment-coefficient curves are nonlinear and indicate a small degree of instability at zero lift about the 50-percent M.A.C. center-of-gravity position and a definite degree of stability about the 25-percent M.A.C. center-of-gravity position. The shape of the moment curves is such that the longitudinal stability would increase and then decrease with increasing lift.

The lift-curve slope for the B_{12} W_{60} V_1 configuration is the same as that for the B_s W_{60} V_1 configuration, but the longitudinal stability is slightly less.

Configuration B_s W_{60} V_2.- Comparison of the data in figures 9 and 13 shows that the drag of the single-fin and twin-fin configurations are almost identical, however, the lift-curve slope of the twin-fin configuration is 0.002 less than that of the single-fin configuration (0.045), based on the same wing area. This change can be accounted for by consideration of the change in wing area (table I). The change in vertical-fin configuration had a negligible effect on the longitudinal stability.

Configuration B_{12} W_{60} FV_1.- The W_{60} F wing incorporates leading-edge fillets which were designed to decrease the wave drag of the root of the basic W_{60} wing. Comparison of figures 10 and 14 shows that the addition of these fillets had no measurable effect on the drag or lift-curve slope and that the complete model with the W_{60}F wing was less stable longitudinally due to the forward movement of the center of pressure. Either the wave drag was not decreased as expected or the effect was counteracted by the increase in friction drag of the additional surface area and by minor differences in the internal drag.

Configuration B_{12} KW_{60} V_2.- A comparison of the drag curves of figures 10 and 15, neglecting the drag increment due to the change in tail configuration, shows that the drag increment due to the pilot's canopy is approximately 6 percent of the measured drag of the B_{12} KW_{60} V_2 configuration. The lift-curve slope and longitudinal stability were unaffected by the addition of the pilot's canopy.

Tests in Yaw

The data obtained from the yaw tests are shown in figures 16 to

19 inclusive. The variation of drag, side force, and yawing-moment coefficients with angle of yaw for the B_s W_{60} configuration is shown in figure 16. The wing-body combination is definitely directionally unstable, but the addition of the V_1 vertical tail causes the airplane to be directionally stable at least about the 25-percent M.A.C. position. (See fig. 17.) The V_2 vertical-fin configuration was not as effective as the V_1 configuration and did not cause the airplane to be directionally stable. (See fig. 18.)

The B_{12} W_{60} V_1 configuration was directionally unstable about the 25-percent M.A.C. point and the addition of the pilot's canopy caused the airplane to be even more directionally unstable. (See fig. 19.)

Elevator and Rudder Effectiveness

The B_s W_{60} V_1 configuration was tested in pitch with rudder neutral and elevator deflections of 0°, -6.5°, -9.9° and -17.8°; and in yaw with elevators neutral and rudder deflections of 0° and -9°. The B_s W_{60} V_2 configuration was tested in pitch with rudders neutral and elevator deflections of 0° and -10.9°; and in yaw with elevators neutral and rudder deflections of 0° and -9°.

The effect of a detached bow wave, which would occur in flight at certain power settings, on the stability and control of the B_s W_{60} V_1 configuration with -9.9° elevator deflection is shown in figure 20. A 0.875-inch diameter washer was installed between the entrance cone and the inner body of the model with the result that the shock wave originating at the duct lip detached and moved forward onto the entrance cone about half way to the cone tip. The three-component data from this test are shown in figure 20(a). The lift, drag, and pitching-moment data for the configuration with the normal internal flow are shown for comparison in figure 20(b). A comparison of the two figures indicates that there would be no stability or trim change due to the forward movement of the shock wave, but that the minimum drag would increase by 28 percent for the particular condition of internal blockage which was tested.

Figures 21 and 22 show the variation of lift with angle of attack for various elevator deflections for the B_s W_{60} V_1 and B_s W_{60} V_2 configurations, respectively. The data are presented for the B_s W_{60} V_1 configuration at two Reynolds numbers. These data are cross-plotted in figures 23 and 24 to show the variation of lift with elevator deflection.

Figures 25, 26, 27, and 28 show the variation of pitching moment with angle of attack for the various elevator deflections for the

B_s W_{60} V_1 and B_s W_{60} V_2 configurations. In figures 25 and 26 the moments are taken about a point at 50 percent of the M.A.C., in figures 27 and 28 at 25 percent of the M.A.C. As before the data for the B_s W_{60} V_1 configuration are presented for two Reynolds numbers. The data from these curves are cross-plotted in figures 29, 30, 31, and 32 to show the variation of pitching moment with elevator deflection for the various angles of attack.

The effect of approximately -9° rudder deflection on drag, side force, and yawing moment for the B_s W_{60} V_1 configuration is shown in figure 17. Similar data for the B_s W_{60} V_2 configuration are shown in figure 18. Comparison of the two figures shows that the B_s W_{60} V_1 configuration has the greater rudder effectiveness; the change in 25 percent M.A.C. yawing-moment coefficient per degree of rudder deflection being approximately -0.0003 for the B_s W_{60} V_1 configuration and -0.0002 for the B_s W_{60} V_2 configuration.

The wing-elevator combination and the vertical fin-rudder combination of the airplane tested in this investigation are very similar in that they are both triangular plan-form airfoils with constant-chord flaps. Therefore, the aerodynamic characteristics should be similar and any theoretical treatment that can be applied to one should be equally applicable to the other.

Considering the elevators, inspection of the curves reveals that both lift and pitching moments exhibit a variation with angle of attack that is essentially linear. The rate of variation appears to be independent of elevator deflection. Lift and moment also vary linearly with elevator deflection up to a deflection angle of approximately 13°. Above this angle of deflection the effectiveness of the elevator decreases. This critical angle can be predicted from the characteristics of two-dimensional oblique shock waves.

It can be shown that an oblique shock wave cannot exist beyond a certain limiting flow deflection angle, which is a function of the stream Mach number. Therefore it would be expected that when the elevator is deflected sufficiently to produce the critical flow deflection angle, the oblique shock at the leading edge of the elevator would detach and become a normal shock wave ahead of the elevator. Calculations indicated that the shock wave detachment would occur at 12.5° elevator deflection at a Mach number of 1.53.

The commonly used parameters of elevator effectiveness that can be evaluated from the data obtained in this investigation are the slope of the lift-elevator deflection curve $\frac{\partial C_L}{\partial \delta_e}$ and the slope

of the pitching-moment elevator-deflection curve $\frac{\partial C_m}{\partial \delta_e}$. A third parameter α_δ may be obtained by dividing $\frac{\partial C_L}{\partial \delta_e}$ by the lift-curve slope $\frac{\partial C_L}{\partial \alpha}$. These slopes were measured at $\delta_e = 0^\circ$ but, because of the linear nature of the curves of the basic data, the values tabulated below may be assumed to apply over the entire angle-of-attack range investigated and for elevator deflections up to 12°.

The effectiveness of the constant-chord elevator for the complete triangular wing can be predicted very closely by an application of Ackeret's theory. (See reference 7.) The application of this theory depends on two assumptions: (a) that the elevator is essentially a rectangular flat plate with no end effects, and (b) that no interaction occurs between the elevators and the wing. With these assumptions, the change in lift due to the elevator deflection is given by the following equation:

$$\left(\Delta C_L\right)_e = \frac{4\delta_e}{57.3\sqrt{M^2-1}} \frac{S_e}{S}$$

The change in the 50-percent M.A.C. pitching moment is given by:

$$\left(\Delta C_{m_{\frac{c}{4}}}\right)_e = -\frac{2\delta_e}{57.3\sqrt{M^2-1}} \frac{S_e}{S}\left(1-\frac{S_e}{S}\right)$$

Values of the effectiveness parameters obtained are given in the following table:

Configuration	$B_s W_{so} V_2$	$B_s W_{so} V_1$ (Experiment)		$B_s W_{so} V_1$ (Theory)
Reynolds Number	1.13×10^6	0.71×10^6	1.13×10^6	
$\frac{\partial C_L}{\partial \delta_e}$	0.0069	0.0075	0.0087	0.0095
α_δ	.157	.167	.191	.211 *
$\frac{\partial C_{m_{c/2}}}{\partial \delta_e}$	-.0033	-.0037	-.0040	-.0040
$\frac{\partial C_{m_{c/4}}}{\partial \delta_e}$	-.0051	-.0058	-.0060	-.0064

* Experimental $\frac{dC_L}{d\alpha}$ used in determining this value.

Figure 33 shows that the experimental data agree with the theory up to the critical deflection angle discussed previously. The good agreement between theory and experiment is partially due to the compensating effect of neglecting both the loss of lift at the elevator tips and the carry-over of the additional lift onto the fuselage.

The theoretical equations do not include viscosity effects and comparison of the various effectiveness parameters shows that the moment-producing effectiveness $\frac{\partial C_m}{\partial \delta_e}$, which was predicted most closely by theory, varied very little between the two Reynolds numbers at which tests were made. On the other hand there is considerable variation in the lift-producing effectiveness $\frac{\partial C_L}{\partial \delta_e}$ with Reynolds number, but the trend is such that the theory should more closely predict the measured value as the test Reynolds number increases toward full-scale values.

A comparison of the effectiveness parameters in the foregoing table, based on the area of the full triangular wing, indicates that the installation of wing-tip fins had an adverse effect. When the changes in wing and elevator areas are considered, however, the elevator effectiveness is unchanged.

CONCLUDING REMARKS

The effectiveness of constant-chord trailing-edge elevators on a triangular plan-form wing was found to be independent of angle of attack through the range investigated and the effectiveness was found to vary linearly with elevator deflection up to a critical angle which could be predicted. It was also found that the elevator effectiveness increased somewhat with increasing Reynolds number with corresponding improvement in the agreement between experimental and theoretical elevator effectiveness.

All the models tested were longitudinally stable with the center of gravity located at 25 percent of the mean aerodynamic chord. However, with center of gravity in this position, all of the configurations were either directionally unstable or exhibited a degree of stability that appears to be marginal.

The models tested exhibited a variation of drag with lift which was only slightly greater than that predicted by theory. Additional research is necessary to determine whether the indicated forward

rotation of the resultant force vector is due to the airfoil section characteristics or to favorable wing-body interaction.

Ames Aeronautical Laboratory,
National Advisory Committee for Aeronautics,
Moffett Field, Calif.

REFERENCES

1. Jones, Robert T.: Properties of Low-Aspect-Ratio Pointed Wings at Speeds Below and Above the Speed of Sound. NACA TN No. 1032, 1946.

2. Puckett, Allen E.: Supersonic Wave Drag of Thin Airfoils. Jour. of Aero. Sci., vol. 13, no. 9, Sept. 1946.

3. Vincenti, Walter G., Nielsen, Jack N., and Matteson, Frederick G.: Investigation of Wing Characteristics at a Mach Number of 1.53. I - Triangular Wings of Aspect Ratio 2. NACA CRM No. A7I10, 1947.

4. Rathert, George A., Jr. and Cooper, George E.: Wing-Flow Tests of a Triangular Wing of Aspect Ratio Two. I - Effectiveness of Several Types of Trailing-Edge Flaps on Flat-Plate Models. NACA CRM No. A7G18, 1947.

5. Van Dyke, Milton D.: Aerodynamic Characteristics Including Scale Effect of Several Wings and Bodies Alone and in Combination at a Mach Number of 1.53. NACA CRM No. AGK22, 1946.

6. Taylor, G. I. and Maccoll, J. W.: The Air Pressure on a Cone Moving at High Speeds. Proc. Royal Society, vol. 139, issue no. A838, Feb. 1, 1933.

7. Taylor, G. I.: Applications to Aeronautics of Ackeret's Theory of Aerofoils Moving at Speeds Greater Than That of Sound. R&M. No. 1467, British A.R.C., 1932.

TABLE I.- MODEL DIMENSIONS

Configuration	$B_sW_{60}V_1$	$B_sW_{60}V_2$
Total wing area, sq in.	13.19	12.72
Total elevator area, sq in.	2.08	1.68
Total vertical fin area, sq in.	2.00[a]	2.05
Total rudder area, sq in.	0.343	0.352
M.A.C. length, in.	3.16	3.28
Span, in.	5.52	4.48
Over-all length, in.	7.35	7.35
Fuselage diameter, in.	1.31	1.31

[a]Including ventral fin.

TABLE II.- INDEX OF FIGURES

Data	Reynolds Number $\times 10^{-6}$	Configurations							
		B_8	B_8W_{60}	$B_8W_{60}V_1$	$B_8W_{60}V_2$	$B_{12}W_{60}V_1$	$B_{12}W_{60}FV_1$	$B_{12}KW_{60}V_2$	$B_{12}KW_{60}V_1$
Variation of lift, drag, and pitching moment with angle of attack with neutral controls.	1.13	7	7 & 8	9	13	10	14	15	
Variation of side force, drag, and yawing moment with angle of yaw.	1.13		16	17	18	19			19
Variation of lift with angle of attack for various elevator deflections.	.71			21a					
	1.13			21b	22				
Variation of lift with elevator deflection angle.	.71			23a					
	1.13			23b	24				
Variation of 50-percent M.A.C. pitching moment with angle of attack for various elevator deflections.	.71			25a					
	1.13			25b	26				
Variation of 25-percent M.A.C. pitching moment with angle of attack for various elevator deflections.	.71			27a					
	1.13			27b	28				
Variation of 50-percent M.A.C. pitching moment with elevator deflection.	.71			29a					
	1.13			29b	30				
Variation of 25-percent M.A.C. pitching moment with elevator deflection.	.71			31a					
	1.13			31b	32				

[redacted]

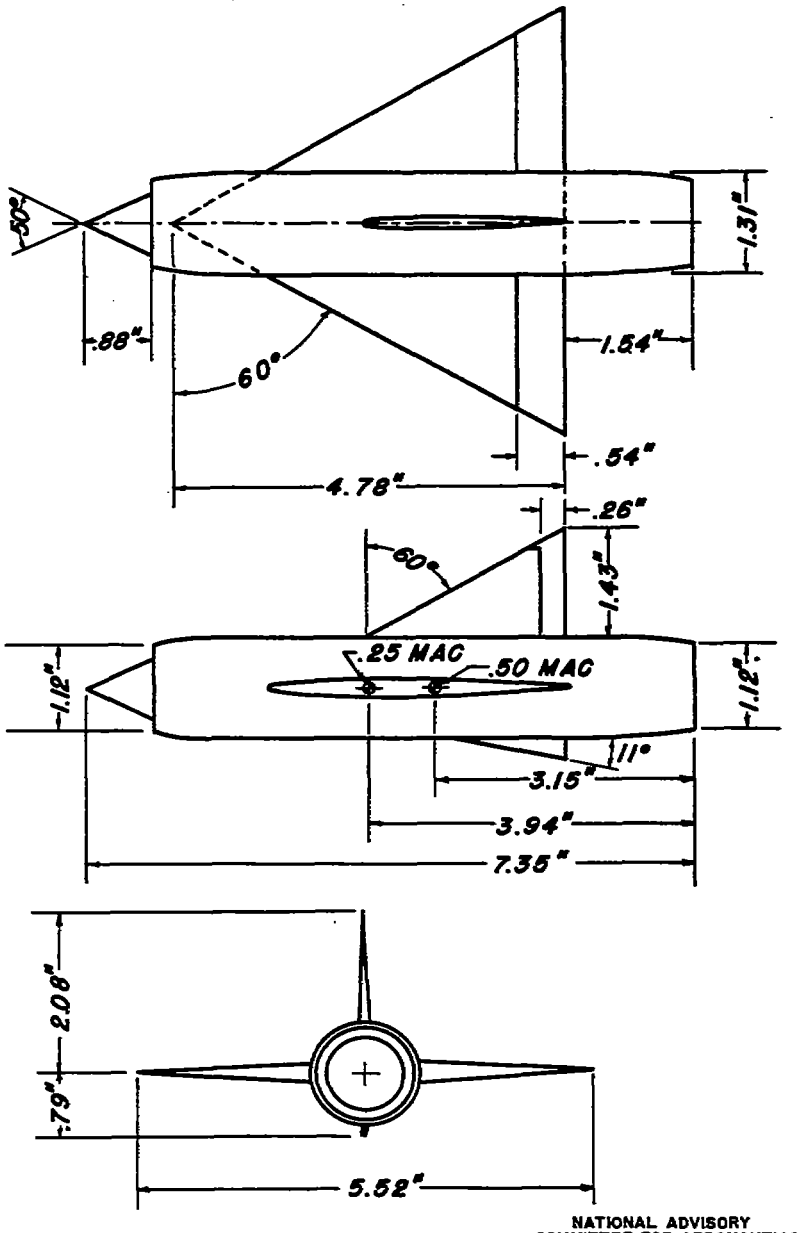

NATIONAL ADVISORY
COMMITTEE FOR AERONAUTICS

(a) Configuration $B_S W_{60} V_1$

Figure 1. - Three-view drawings of the models investigated.

[redacted]

[redacted]

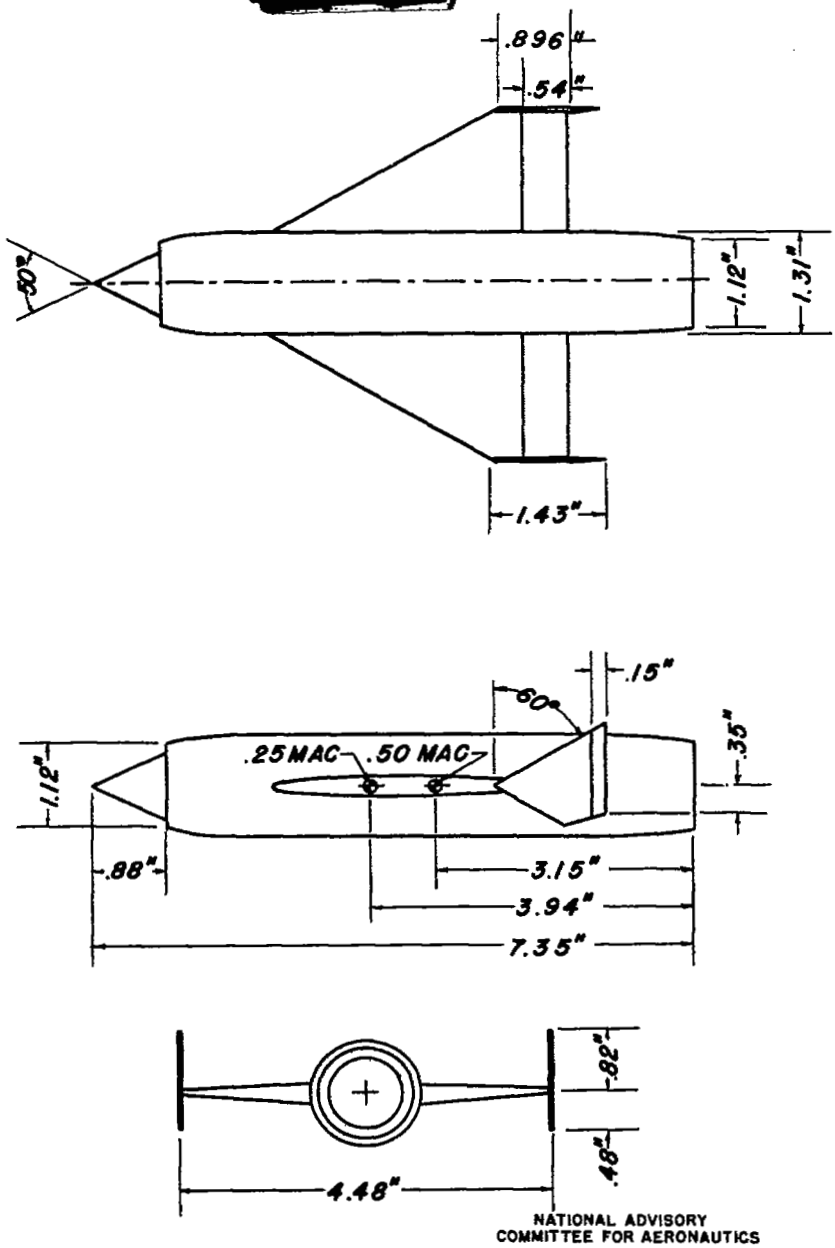

(b) Configuration $B_S W_{60} V_2$

Figure 1.- Continued.

[redacted]

[redacted]

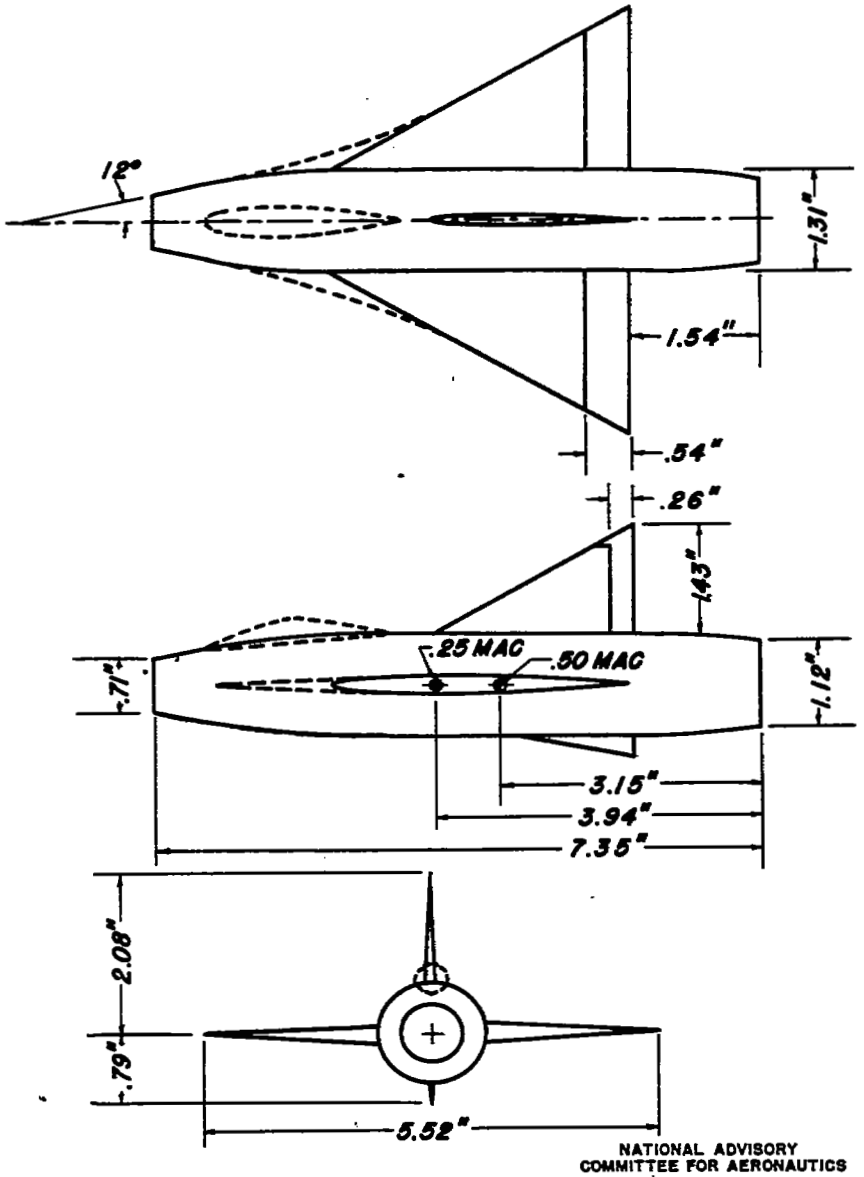

NATIONAL ADVISORY COMMITTEE FOR AERONAUTICS

(c) Configuration $B_{12}W_{60}V_{1}$, K, and F

Figure 1. – Concluded

[redacted]

[redacted]

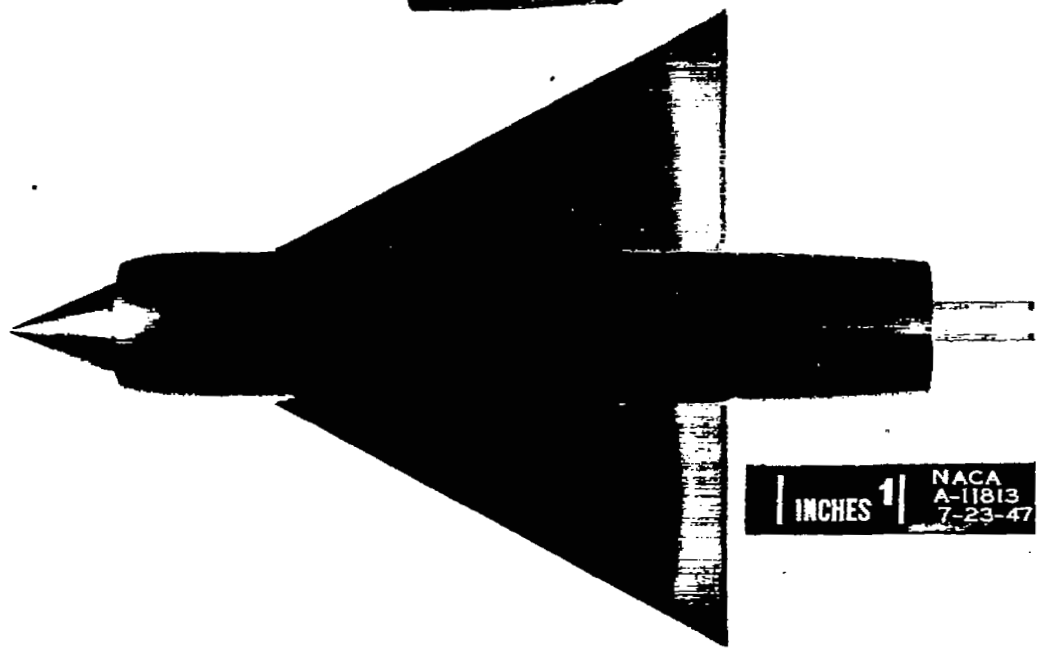

(a) Plan view.

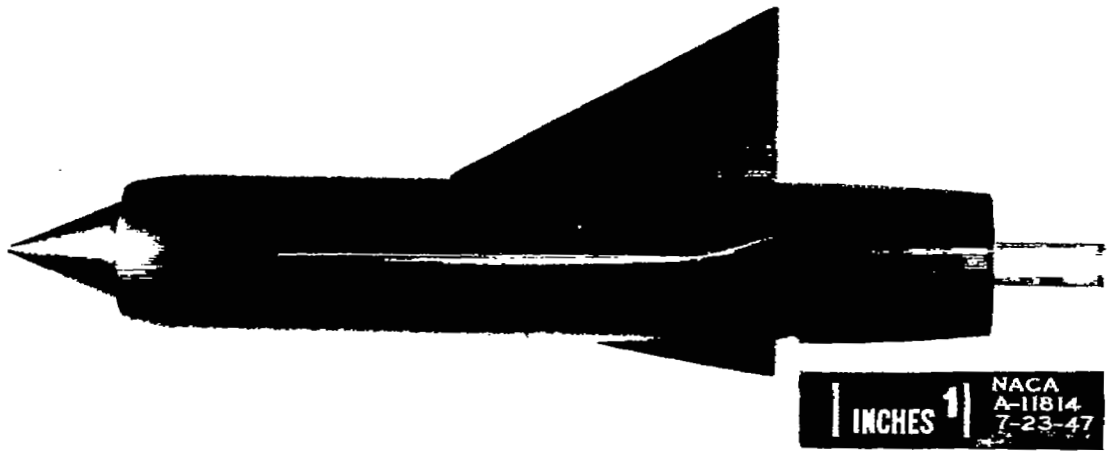

[redacted]

NATIONAL ADVISORY COMMITTEE
FOR AERONAUTICS

(b) Side view.

Figure 2.- The 1/64-scale model of configuration $B_s\ W_{60}\ V_1$ $-\delta_e = 17.8^{\circ}$.

[redacted]

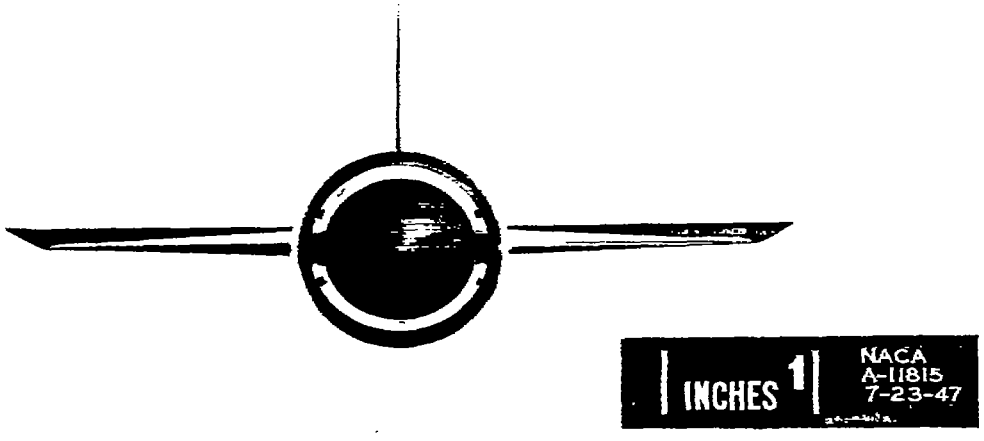

(c) Front view

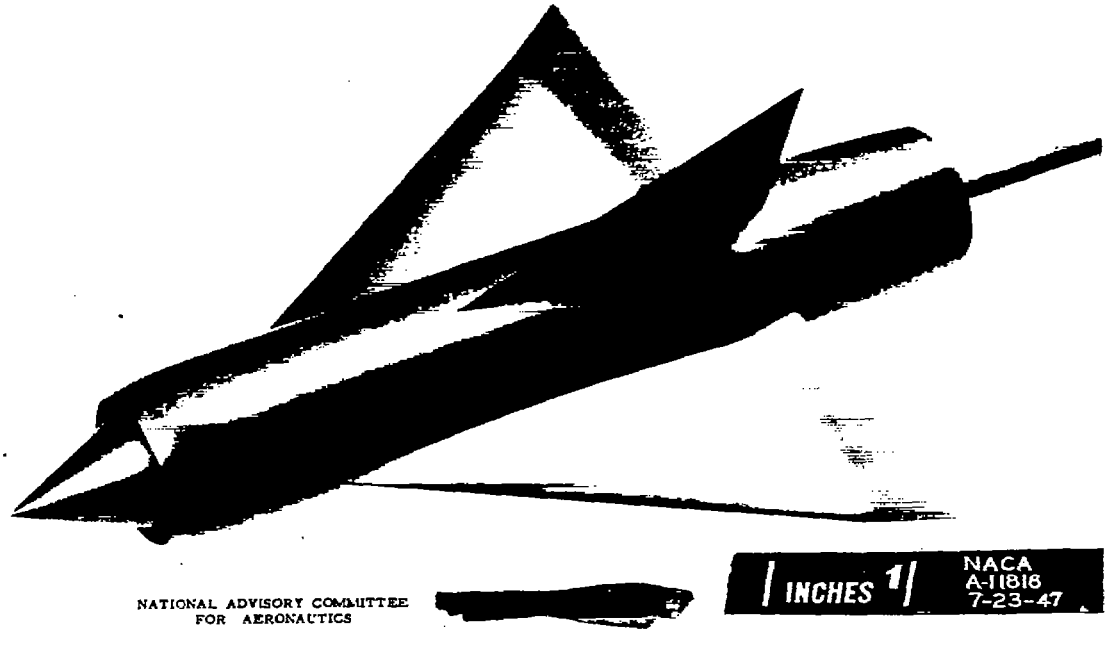

NATIONAL ADVISORY COMMITTEE
FOR AERONAUTICS

[redacted]

(d) Three-quarter view.

Figure 2.- Concluded.

[redacted]

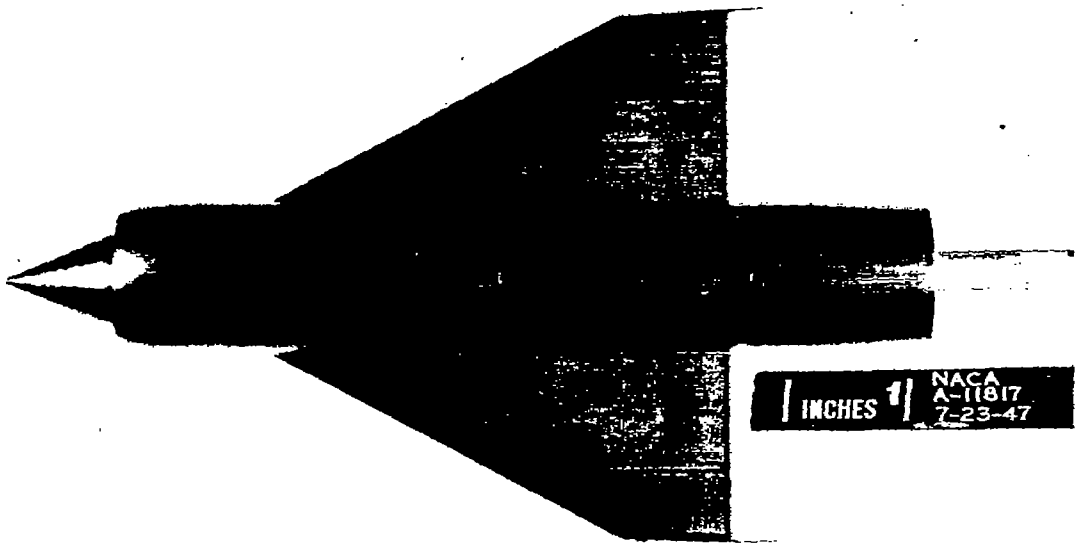

(a) Plan view.

[redacted]

NATIONAL ADVISORY COMMITTEE
FOR AERONAUTICS

(b) Side View.

Figure 3.- The 1/64-scale model of configuration $B_sW_{60}V_2$-δ_e=0°.

(c) Front view.

(d) Three-quarter view

Figure 3.- Concluded.

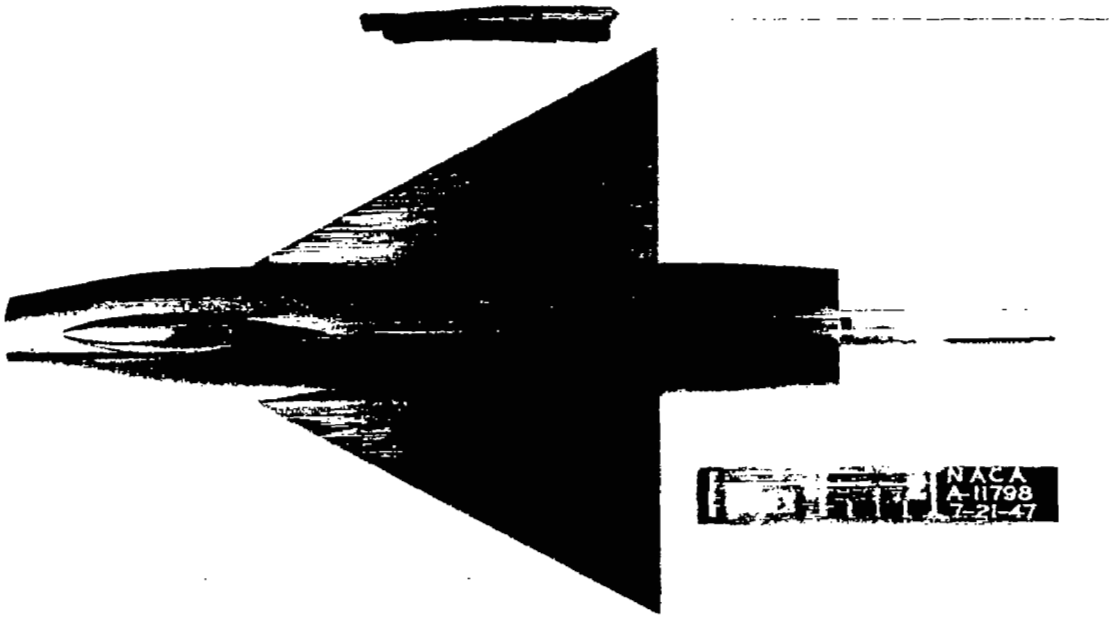

(a) Plan view.

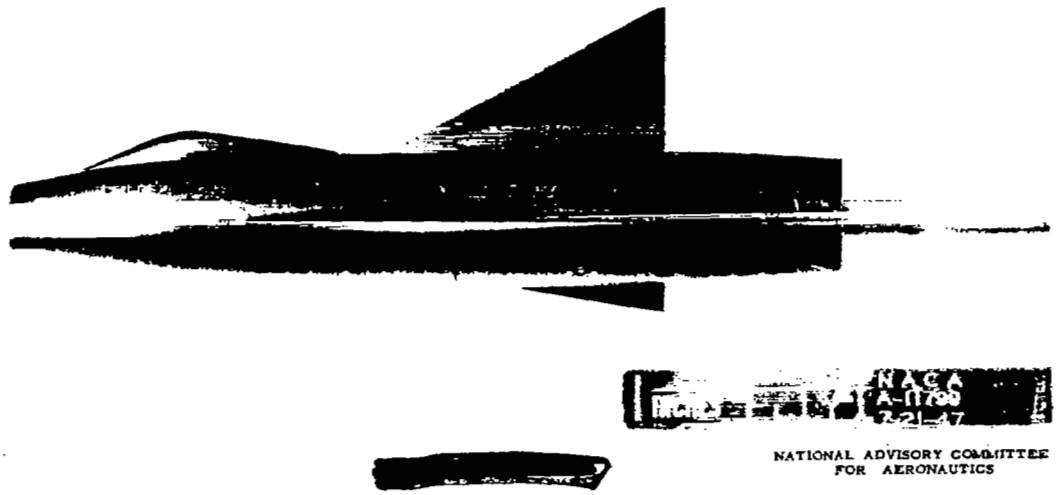

(b) Side view.

Figure 4.- The 1/64-scale model of configuration $B_{12}KW_{60}V_1$-$\delta_e=0^\circ$.

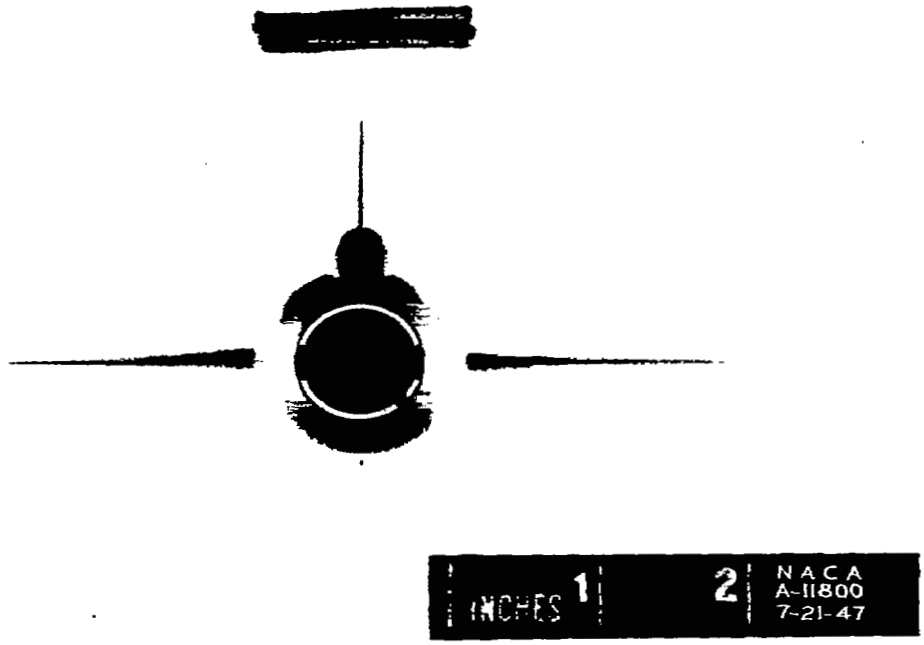

(c) Front view.

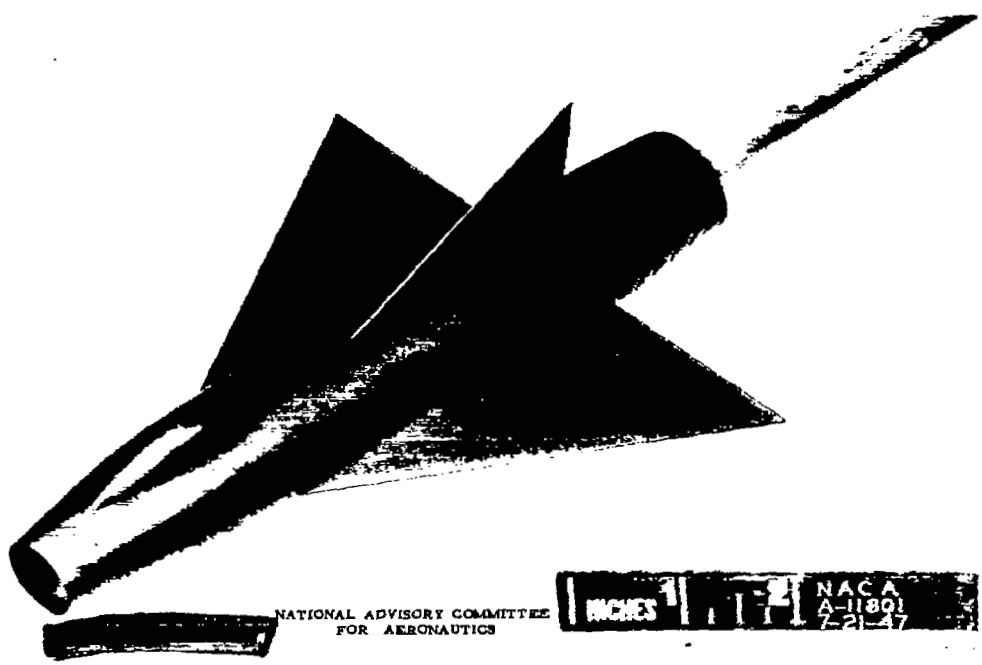

(d) Three-quarter view

Figure 4.- Concluded.

[redacted]

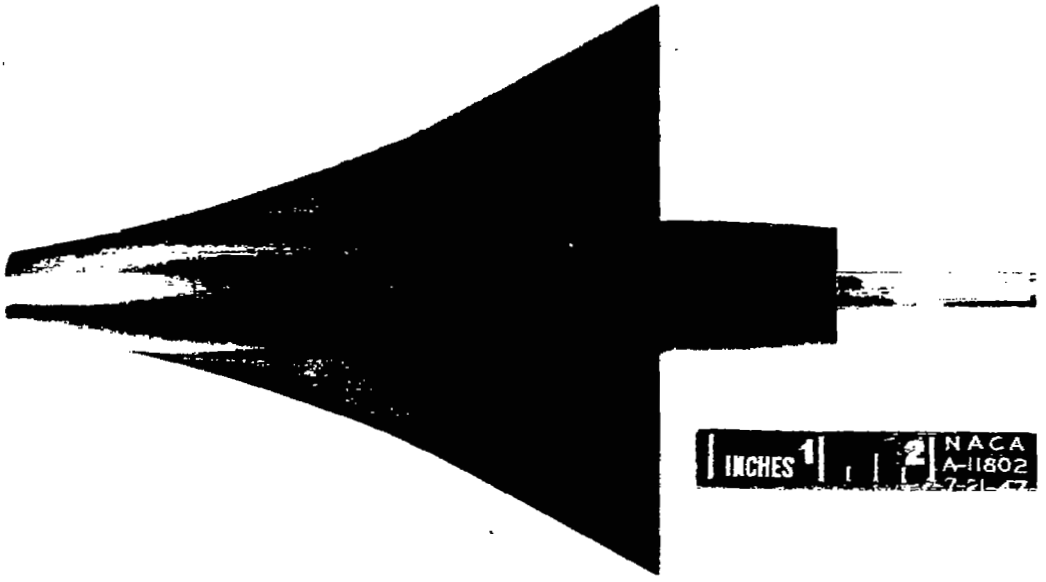

(a) Plan view.

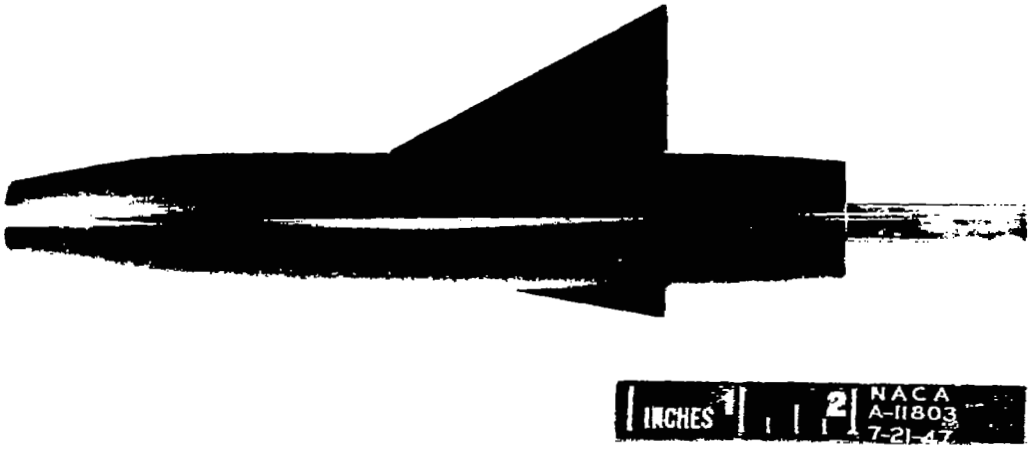

[redacted]

NATIONAL ADVISORY COMMITTEE FOR AERONAUTICS

(b) Side view.

Figure 5.- The 1/64-scale model of configuration $B_{12}W_{60}FV_1$-$\delta_e=0^\circ$.

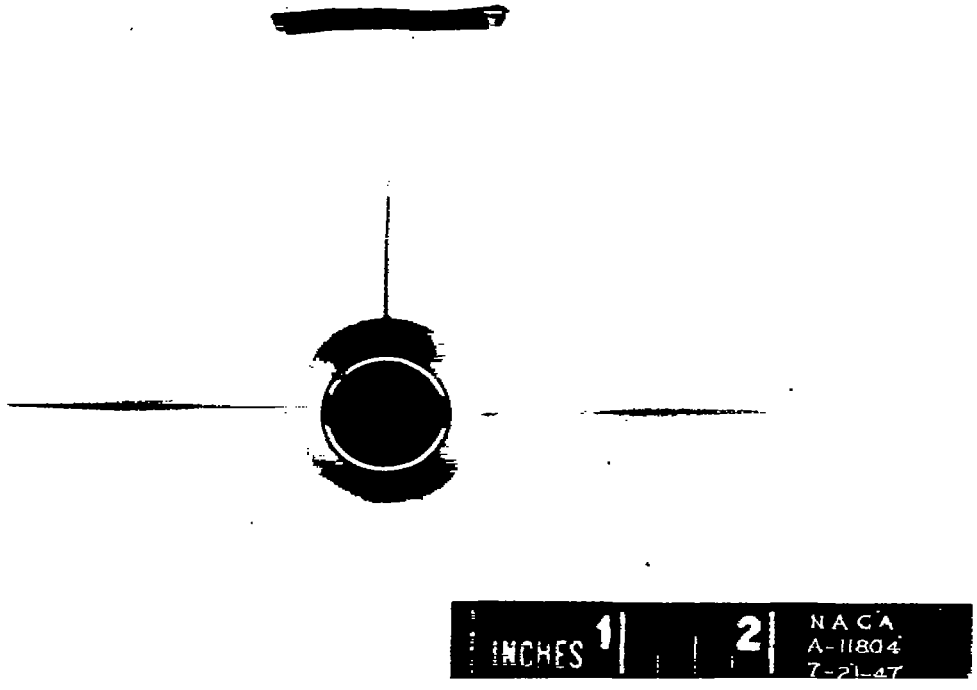

(c) Front view.

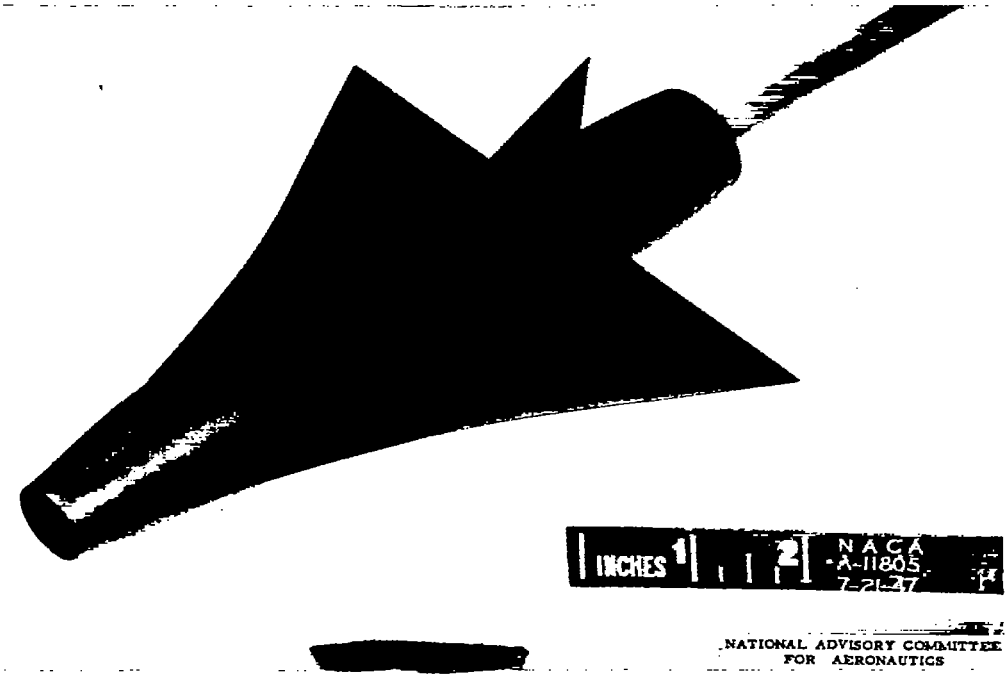

(d) Three-quarter view.

Figure 5.- Concluded.

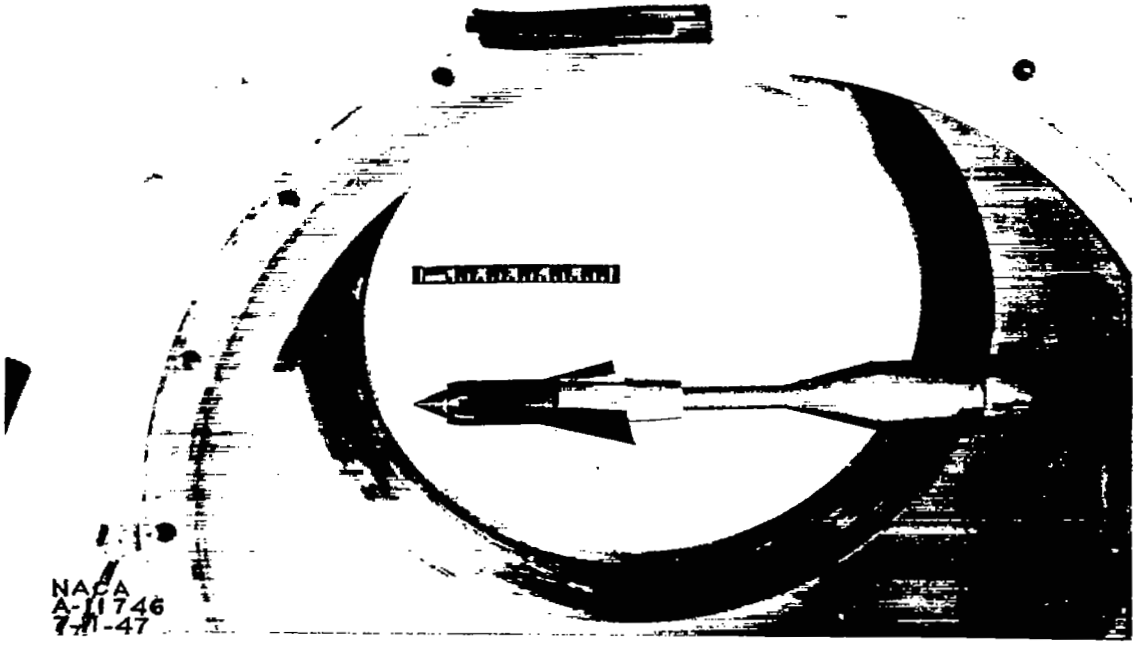

(a) Low angle-of-attack installation.

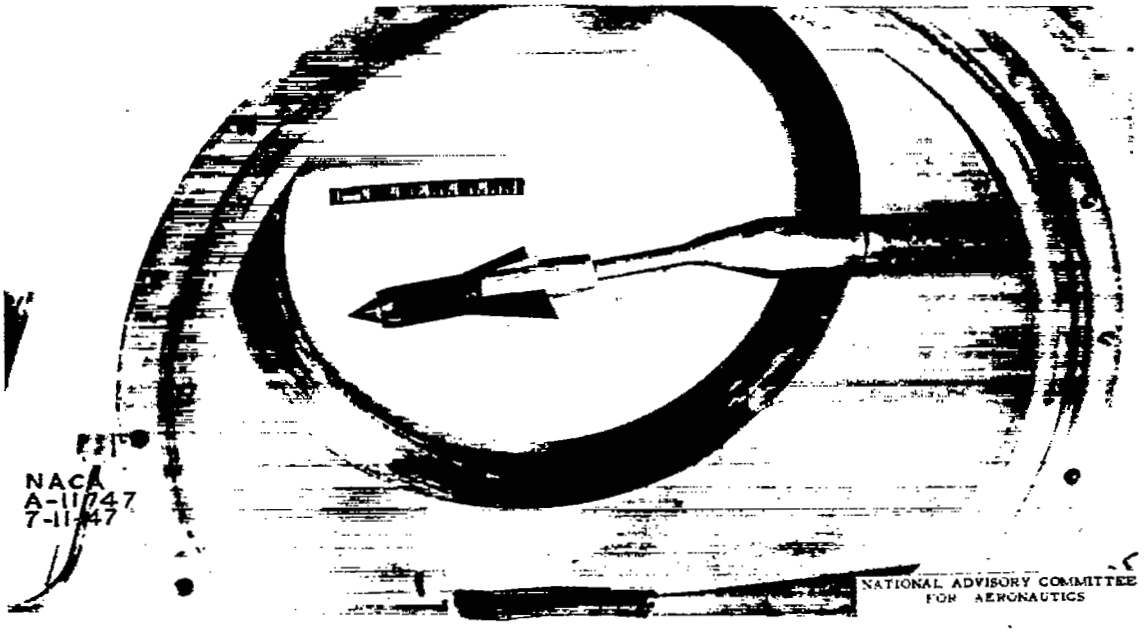

(b) High angle-of-attack installation.

Figure 6.- Configuration $B_sW_{60}V_1$ installed in the Ames 1- by 3-foot supersonic wind tunnel No.1.

[redacted]

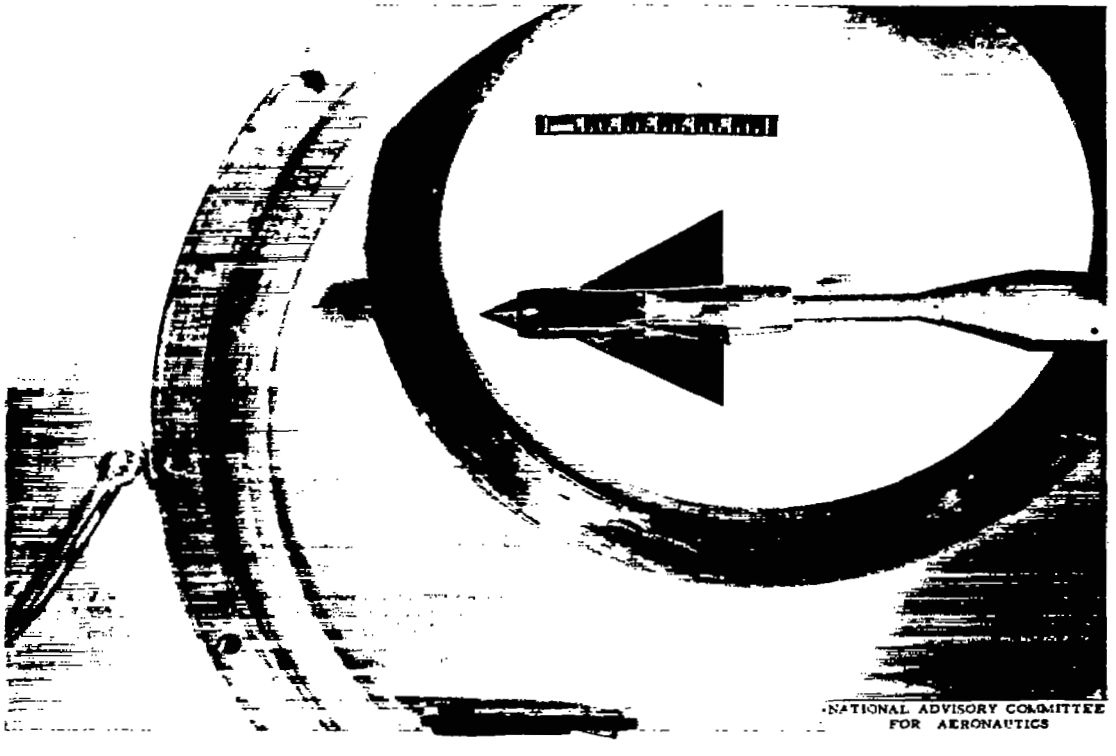

(c) Angle-of-yaw installation.

Figure 6.- Concluded.

[redacted]

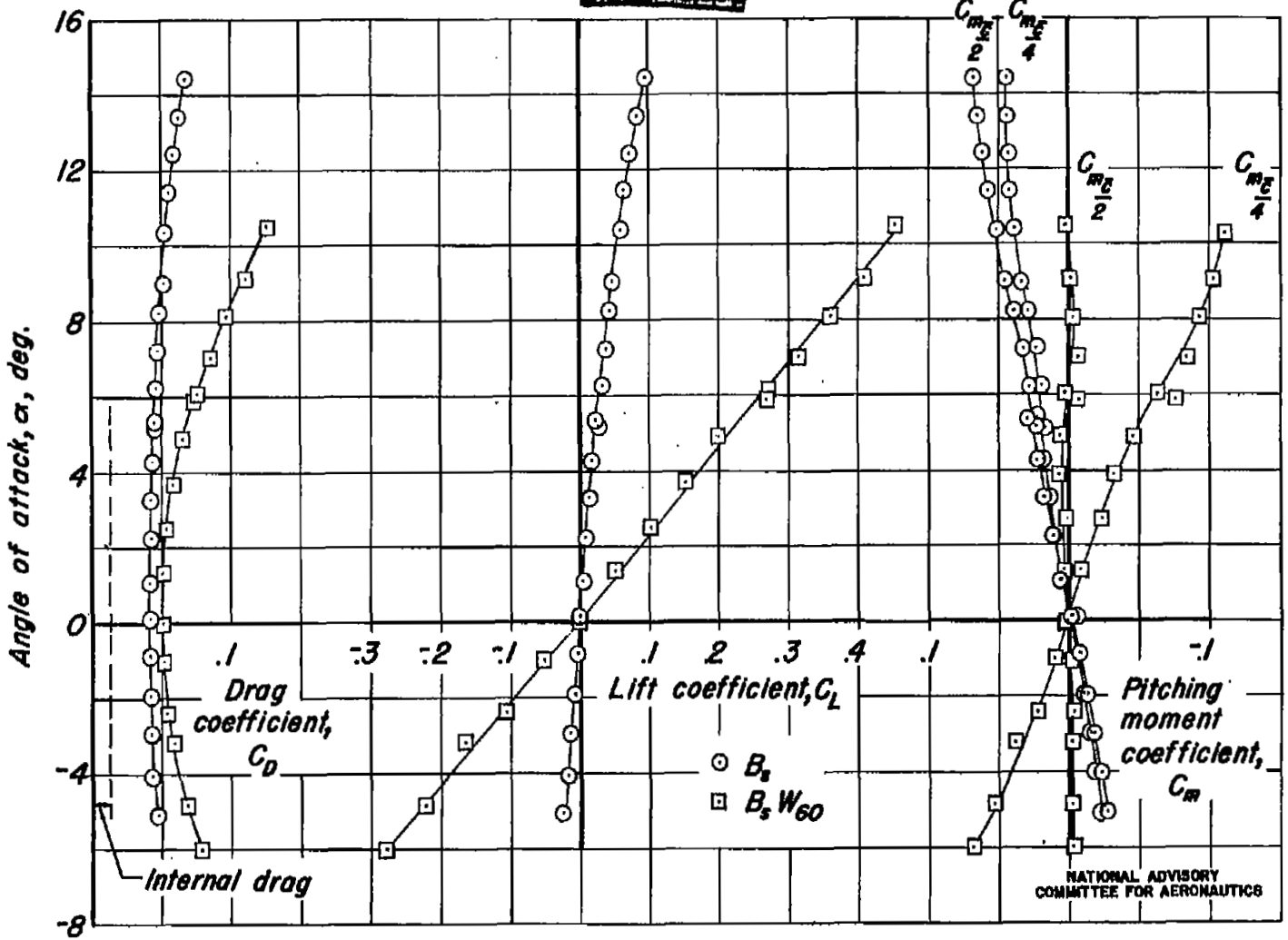

Figure 7.- Variation of drag, lift, and pitching-moment coefficients with angle of attack for the fuselage alone (B_s) and the wing and fuselage ($B_s W_{60}$) at 1.13×10^6 Reynolds number.

[redacted]

[redacted]

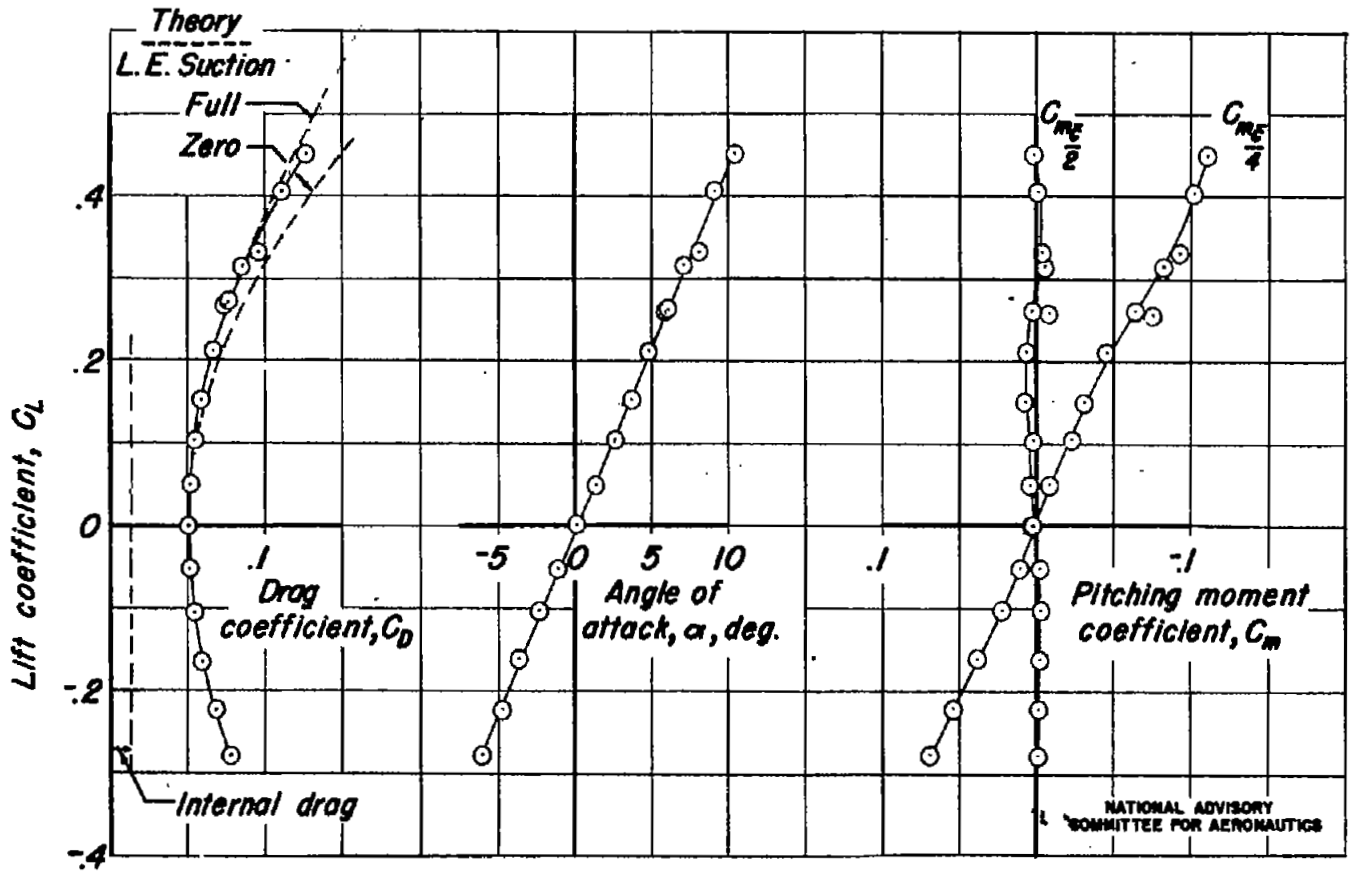

Figure 8.- Variation of drag coefficient, angle of attack, and pitching-moment coefficient with lift coefficient for the wing and fuselage ($B_s W_{60}$) at 1.13×10^6 Reynolds number.

[redacted]

[redacted]

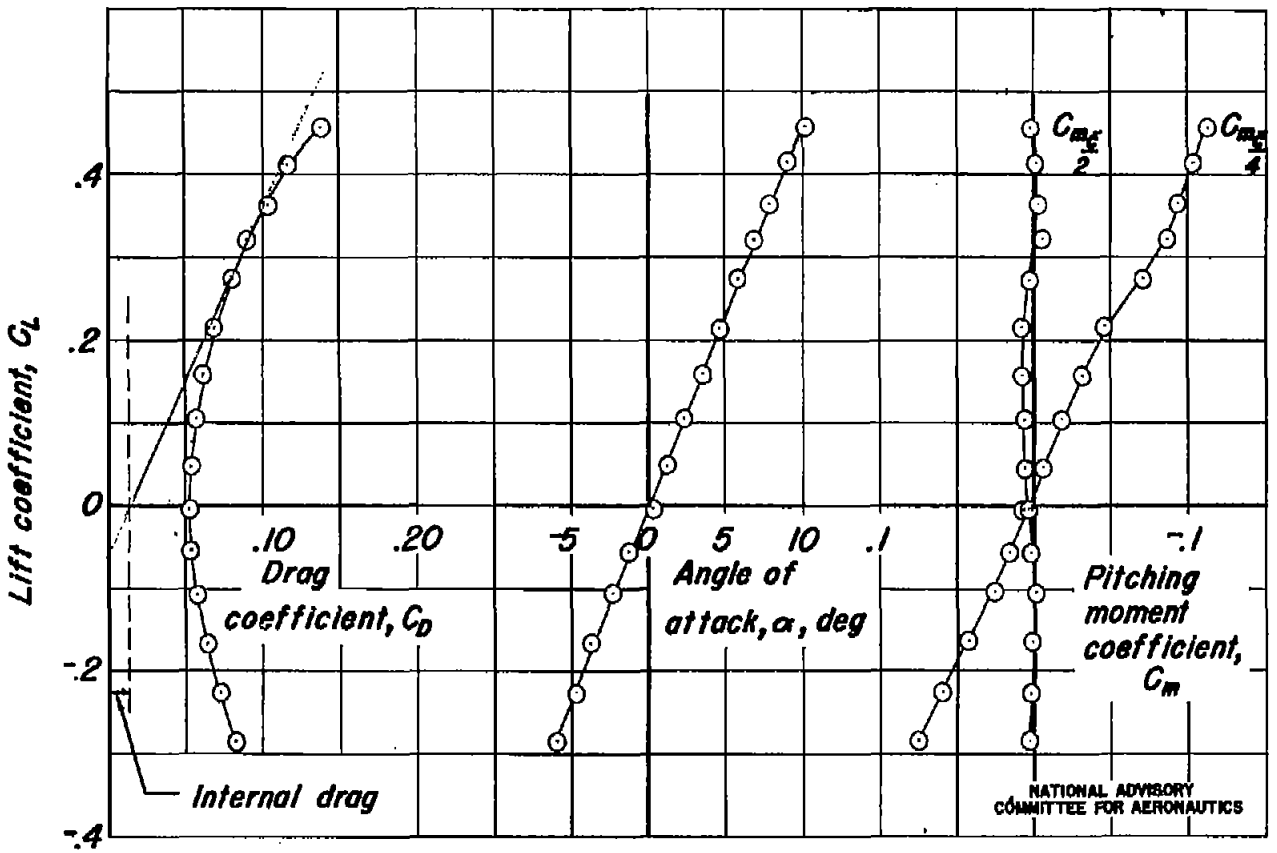

Figure 9.–Variation of drag coefficient, angle of attack, and pitching-moment coefficient with lift coefficient for configuration $B_s W_{60} V_1$ – $\delta_e = 0^\circ$ at 1.13×10^6 Reynolds number.

[redacted]

[redacted]

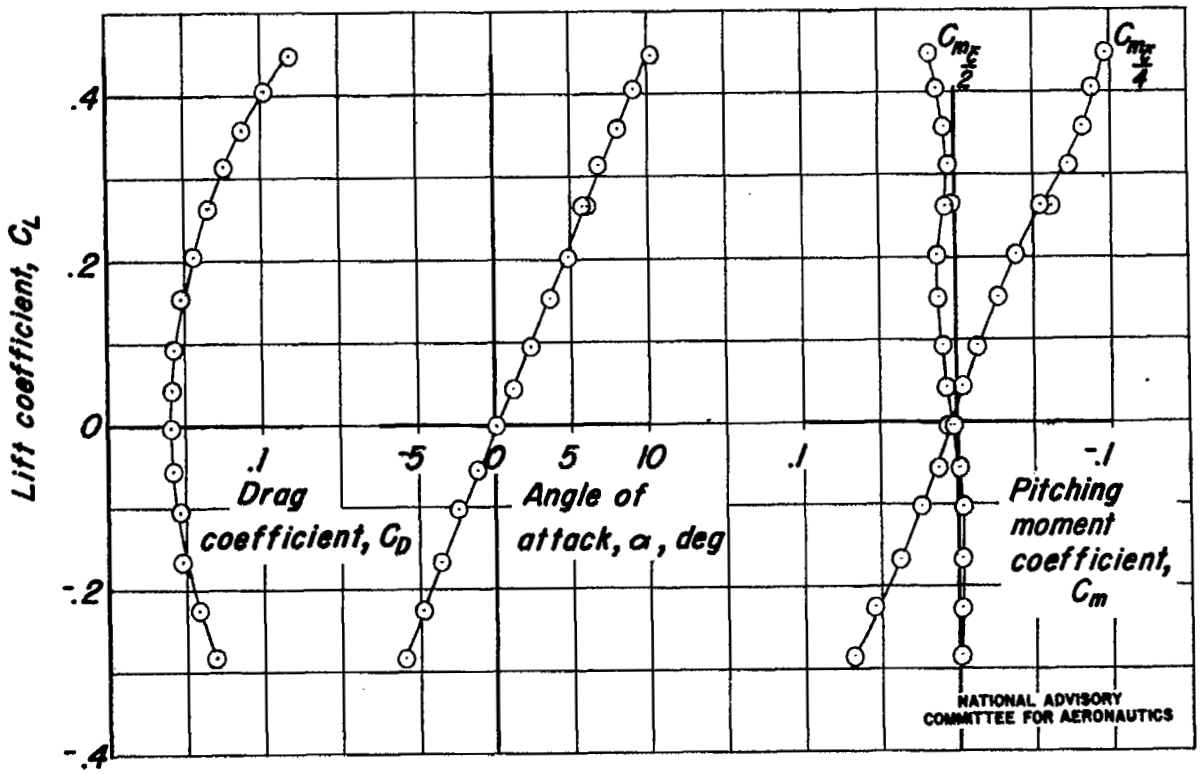

Figure 10.- Variation of drag coefficient, angle of attack, and pitching-moment coefficient with lift coefficient for configuration $B_{12}W_{60}V_1$ - $\delta_e=0^\circ$ at 1.13×10^6 Reynolds number.

[redacted]

Figure 11.- Profile schlieren photograph of configuration $B_{12}W_{60}V_1$ at 1.13×10^6 Reynolds number.

Figure 12.- Profile schlieren photograph of configuration $B_sW_{60}V_1$ at 1.13×10^6 Reynolds number.

[redacted]

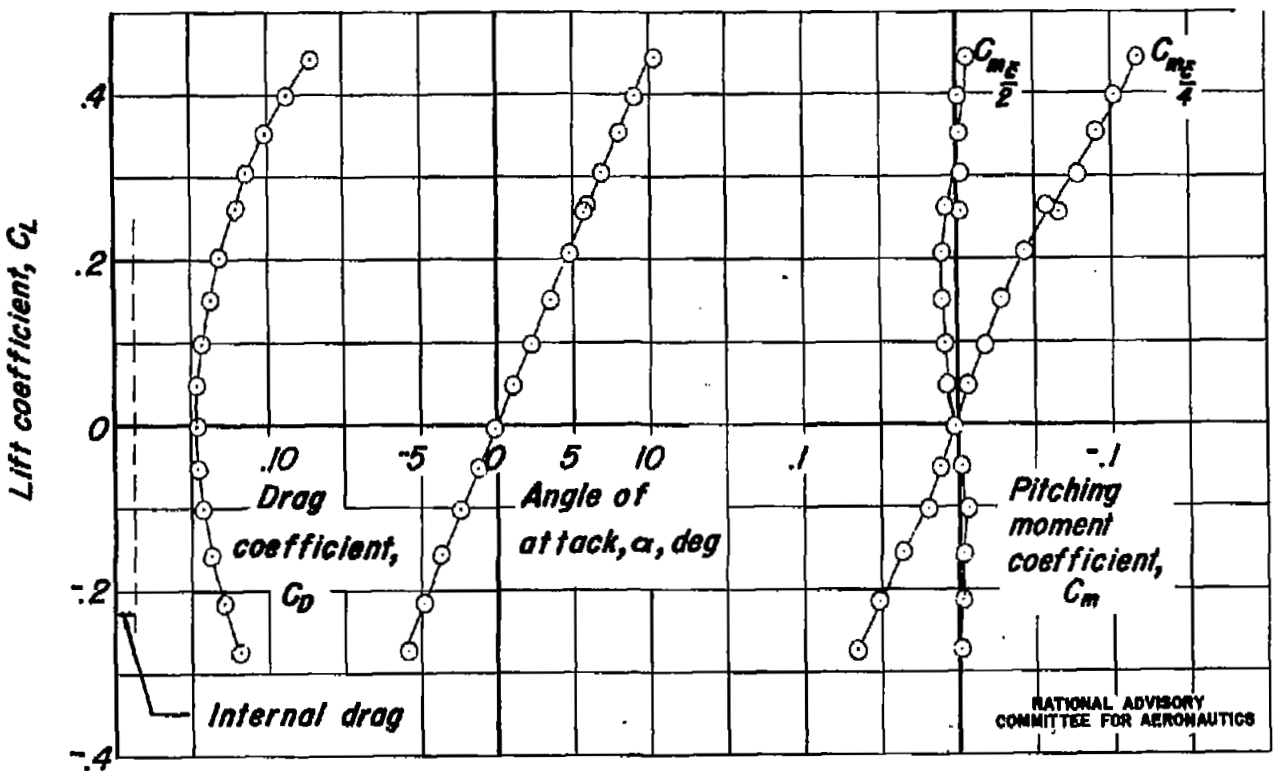

Figure 13.- Variation of drag coefficient, angle of attack, and pitching-moment coefficient with lift coefficient for configuration $B_S W_{60} V_2$ $-\delta_e = 0°$ at 1.13×10^6 Reynolds number.

[redacted]

[redacted]

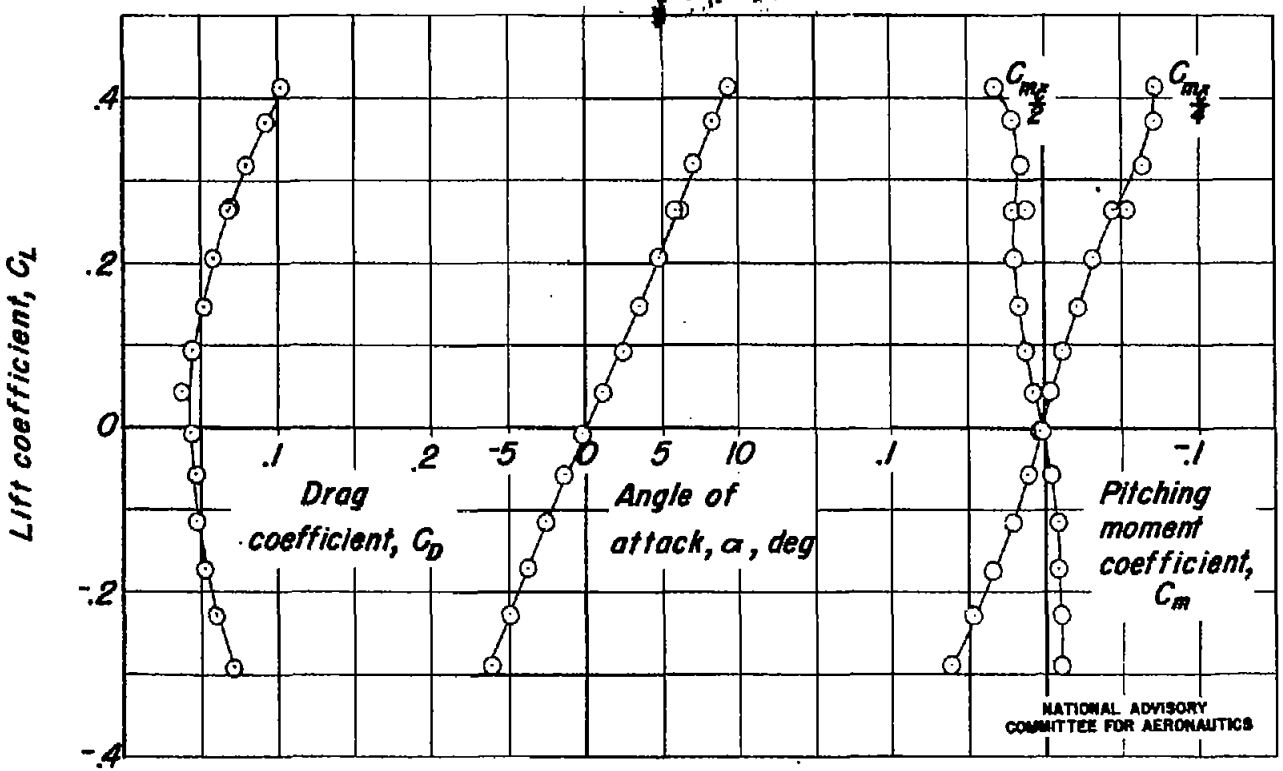

Figure 14. – Variation of drag coefficient, angle of attack, and pitching-moment coefficient with lift coefficient for configuration $B_{12}W_{60}FV_1 - \delta_e = 0°$ at 1.13×10^6 Reynolds number.

[redacted]

[redacted]

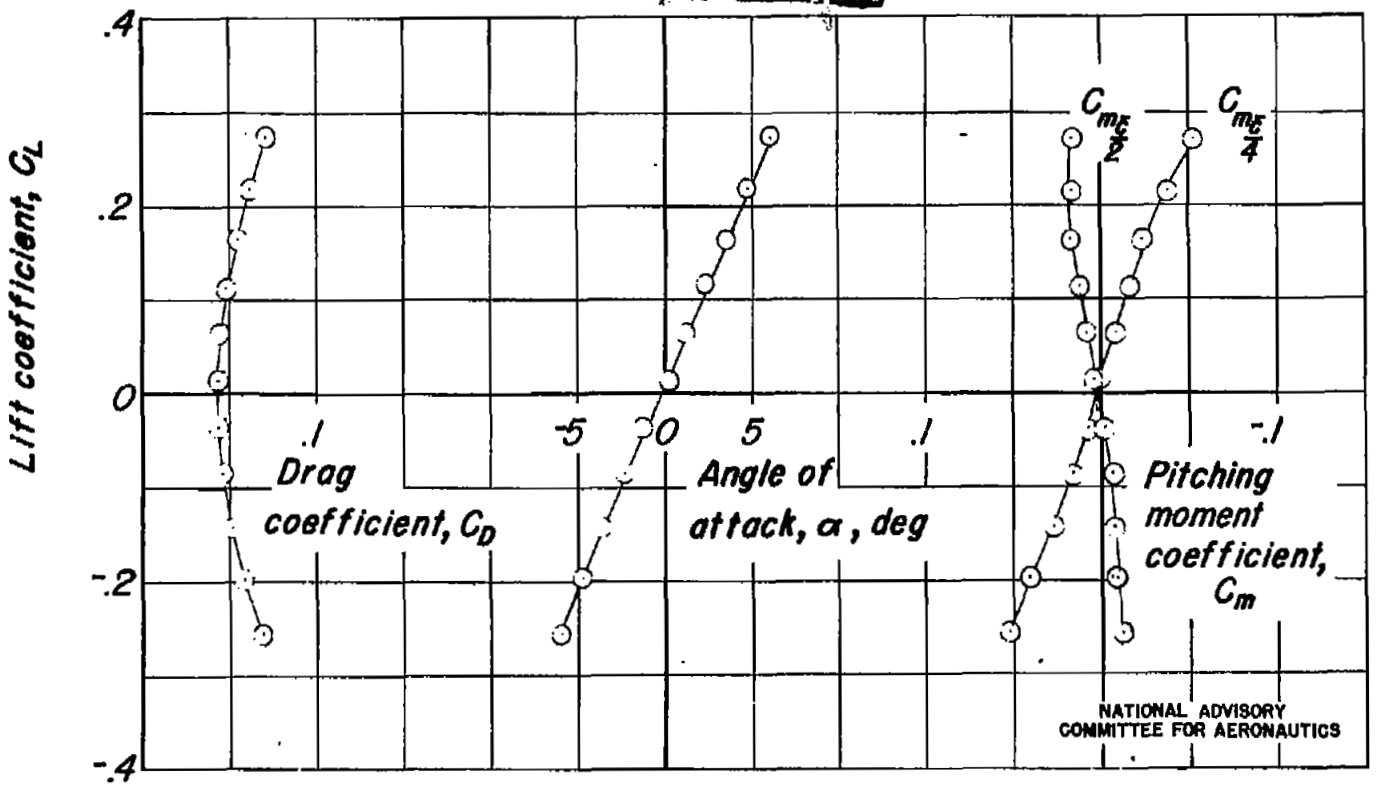

Figure 15. - Variation of drag coefficient, angle of attack, and pitching-moment coefficient with lift coefficient for configuration, B_{12} $KW_{60}V_2$ - $\delta_a = 0°$ at 1.13×10^6 Reynolds number.

[redacted]

[redacted]

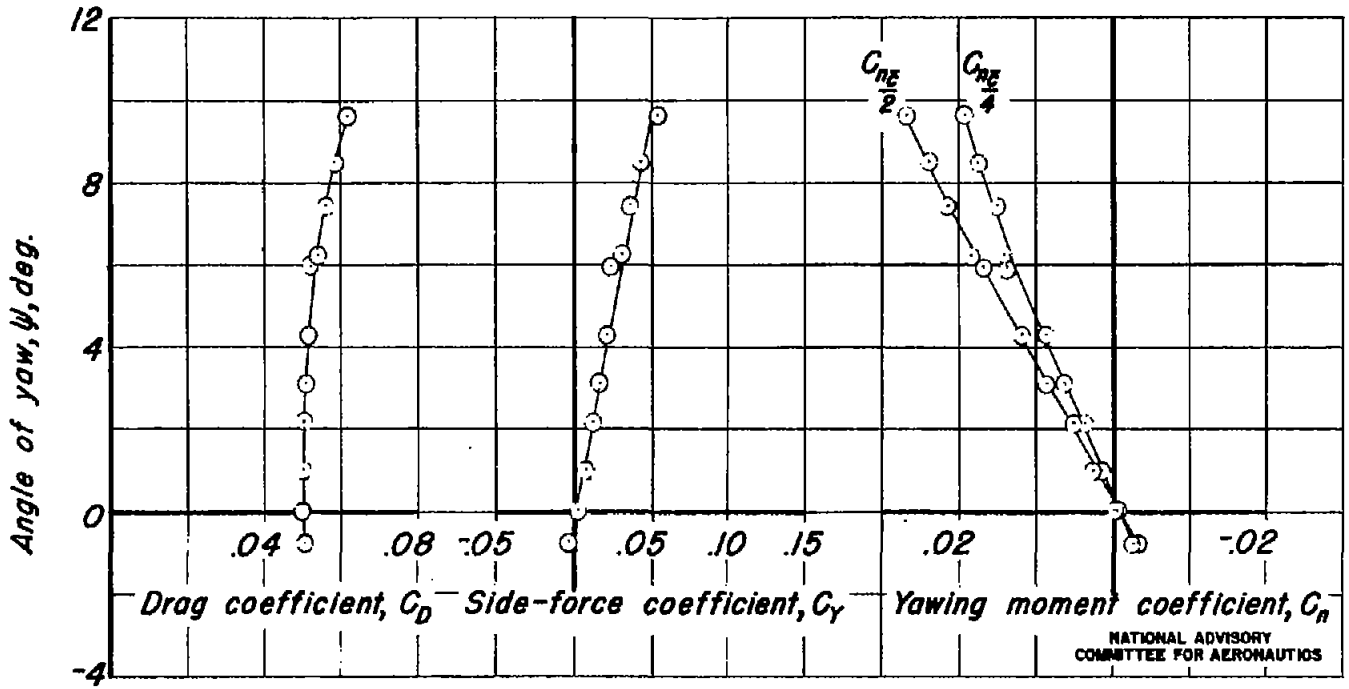

Figure 16.- Variation of drag, side-force, and yawing-moment coefficients with angle of yaw for the wing and fuselage (B_S W_{60}) without vertical fin at 1.13×10^6 Reynolds number.

[redacted]

[redacted]

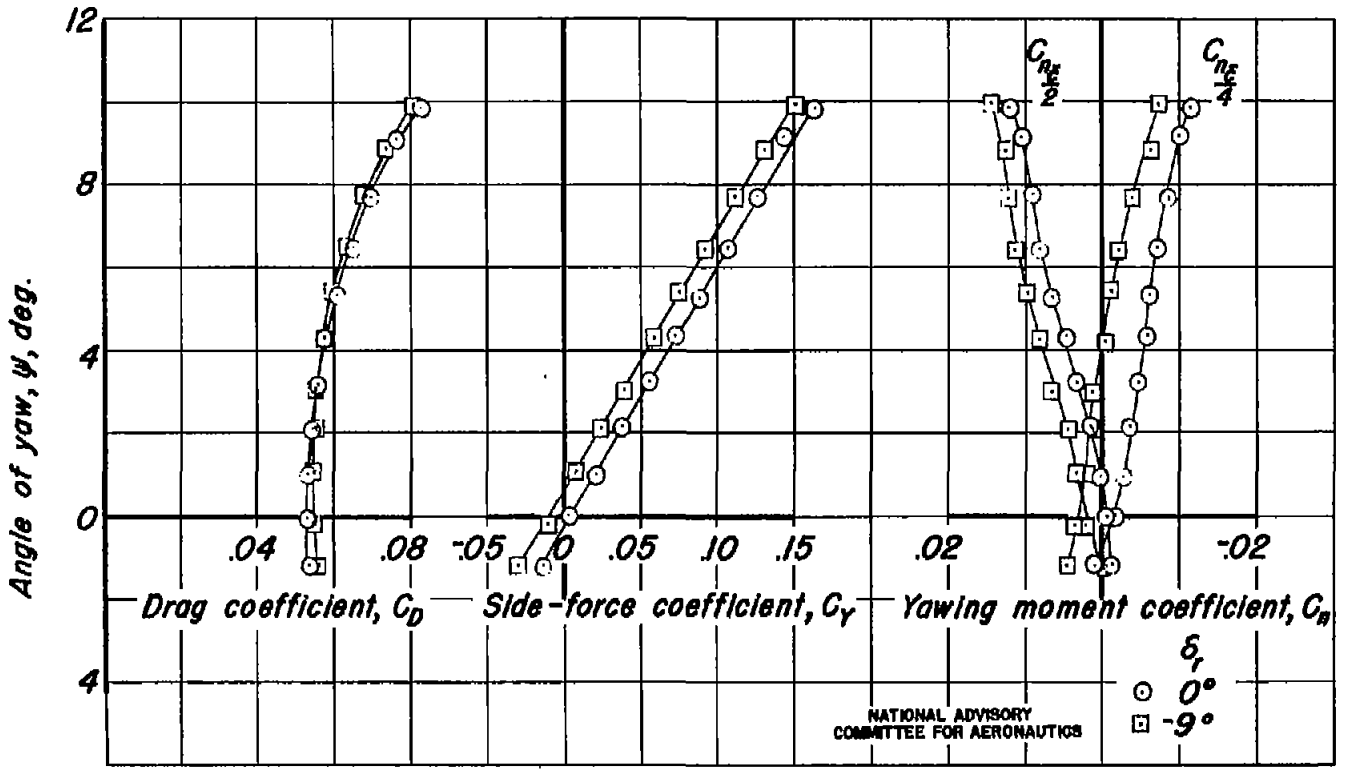

Figure 17. - Variation of drag, side-force, and yawing-moment coefficient with angle of yaw for configuration $B_S W_{60} V_1$ - $\delta_r = 0°$ and -9° at 1.13×10^6 Reynolds number

[redacted]

[redacted]

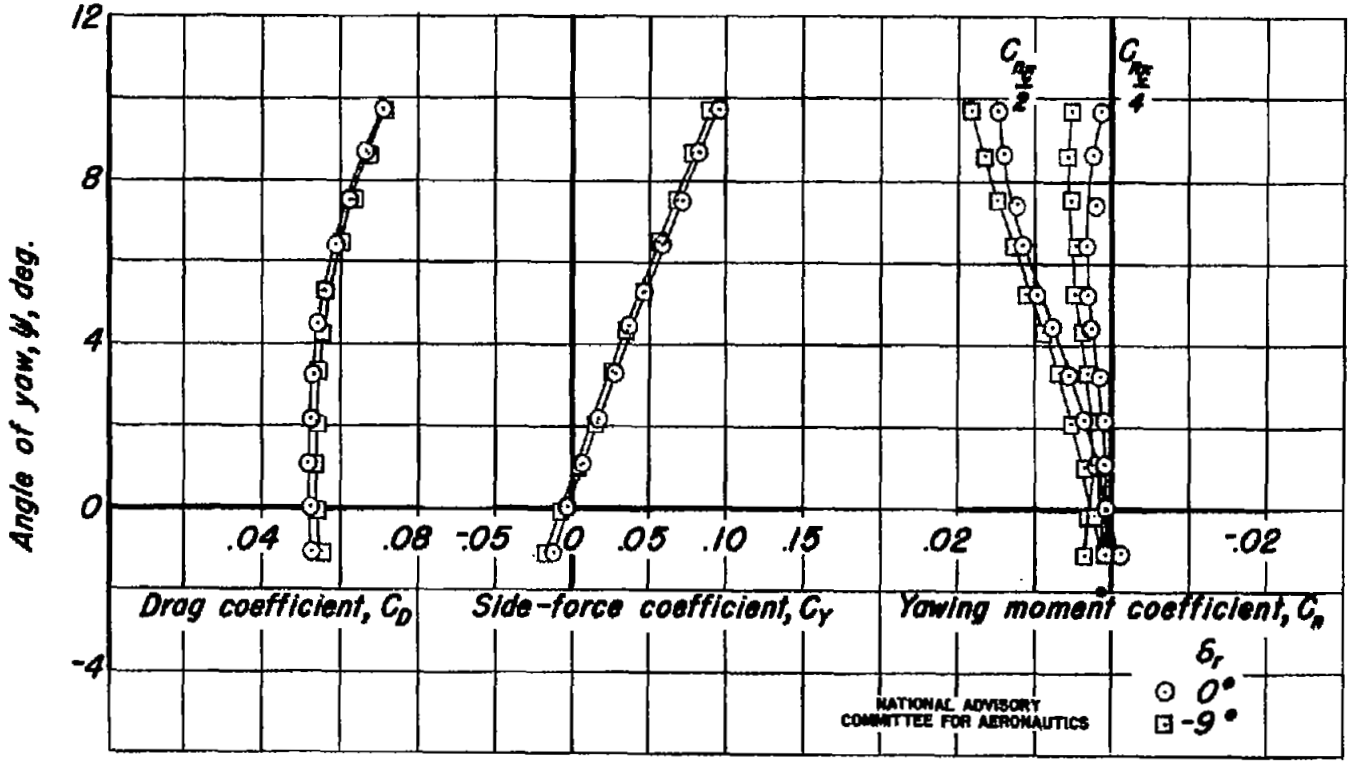

Figure 18.- Variation of drag, side-force, and yawing-moment coefficients with angle of yaw for configuration $B_6W_{60}V_2$ - $\delta_r = 0°$ and -9° at 1.13×10^6 Reynolds number.

[redacted]

[redacted]

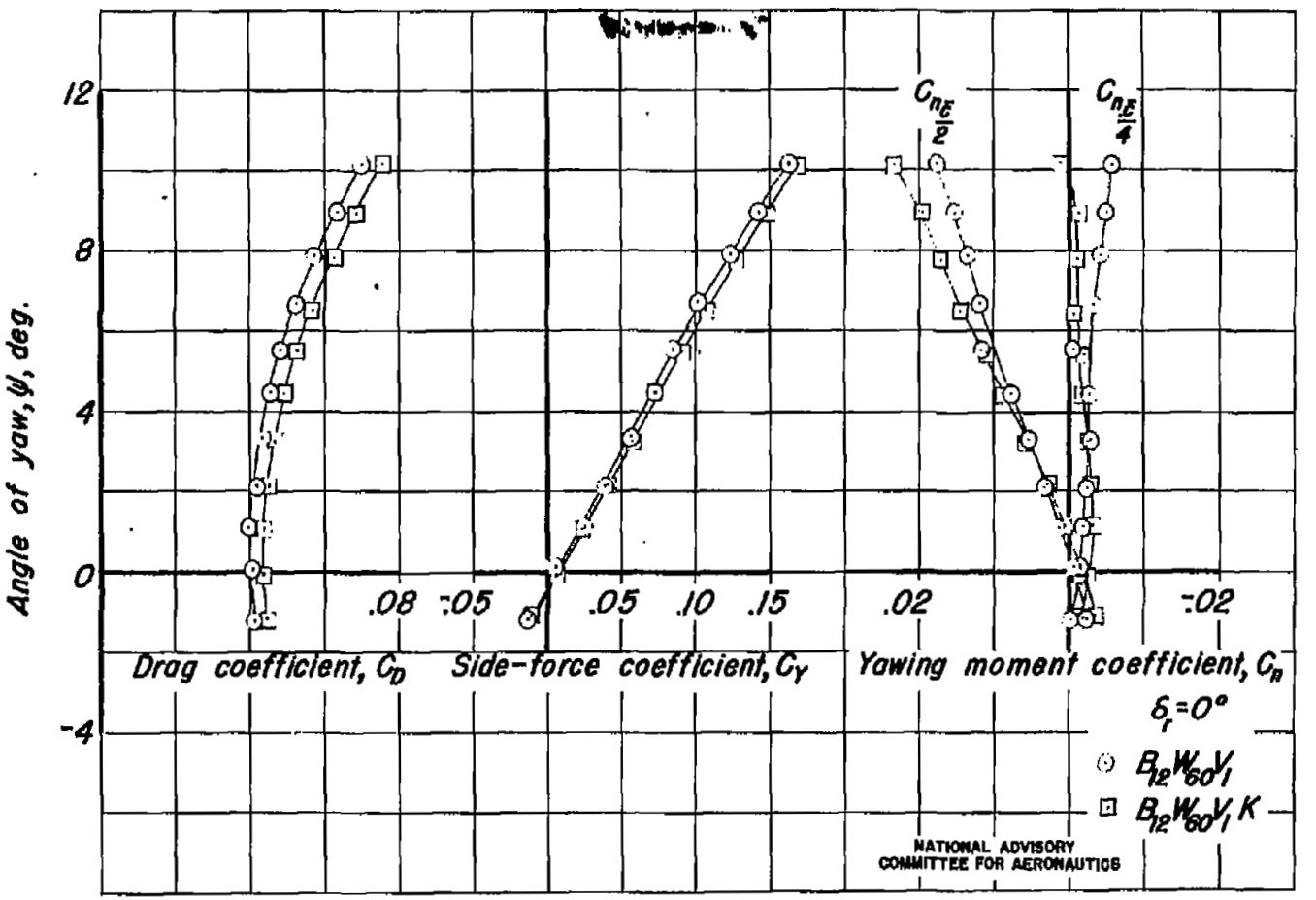

Figure 19.- Variation of drag, side-force, and yawing-moment coefficients with angle of yaw for configurations $B_{12}W_{60}V_1$ and $B_{12}KW_{60}V_1$ - $\delta_r = 0°$ at 1.13×10^6 Reynolds number.

[redacted]

[redacted]

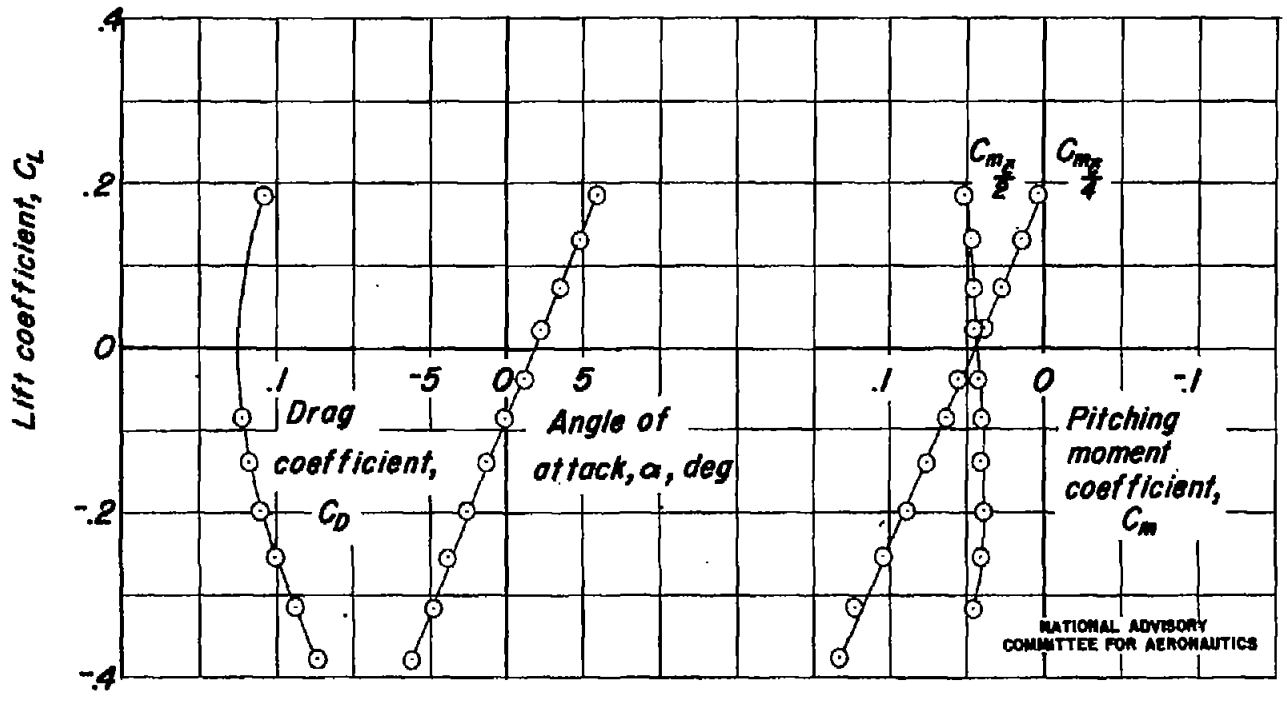

(a) Internal flow partially blocked

Figure 20. - Variation of drag coefficient, angle of attack, and pitching-moment coefficient with lift coefficient for configuration $B_S W_{60} V_1$ - $\delta_e = -9.9°$ at 1.13×10^6 Reynolds number.

[redacted]

[redacted]

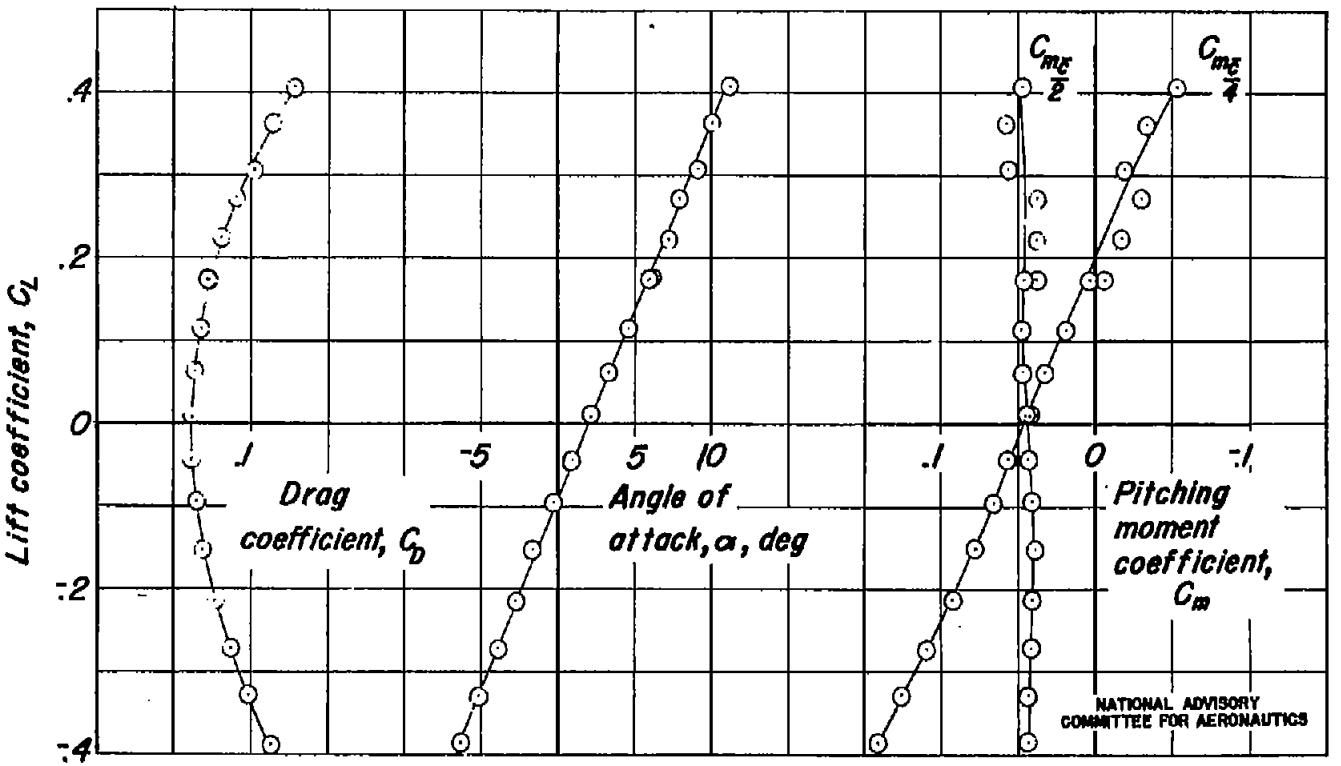

(b) Normal internal flow

Figure 20. - Concluded

[redacted]

[redacted]

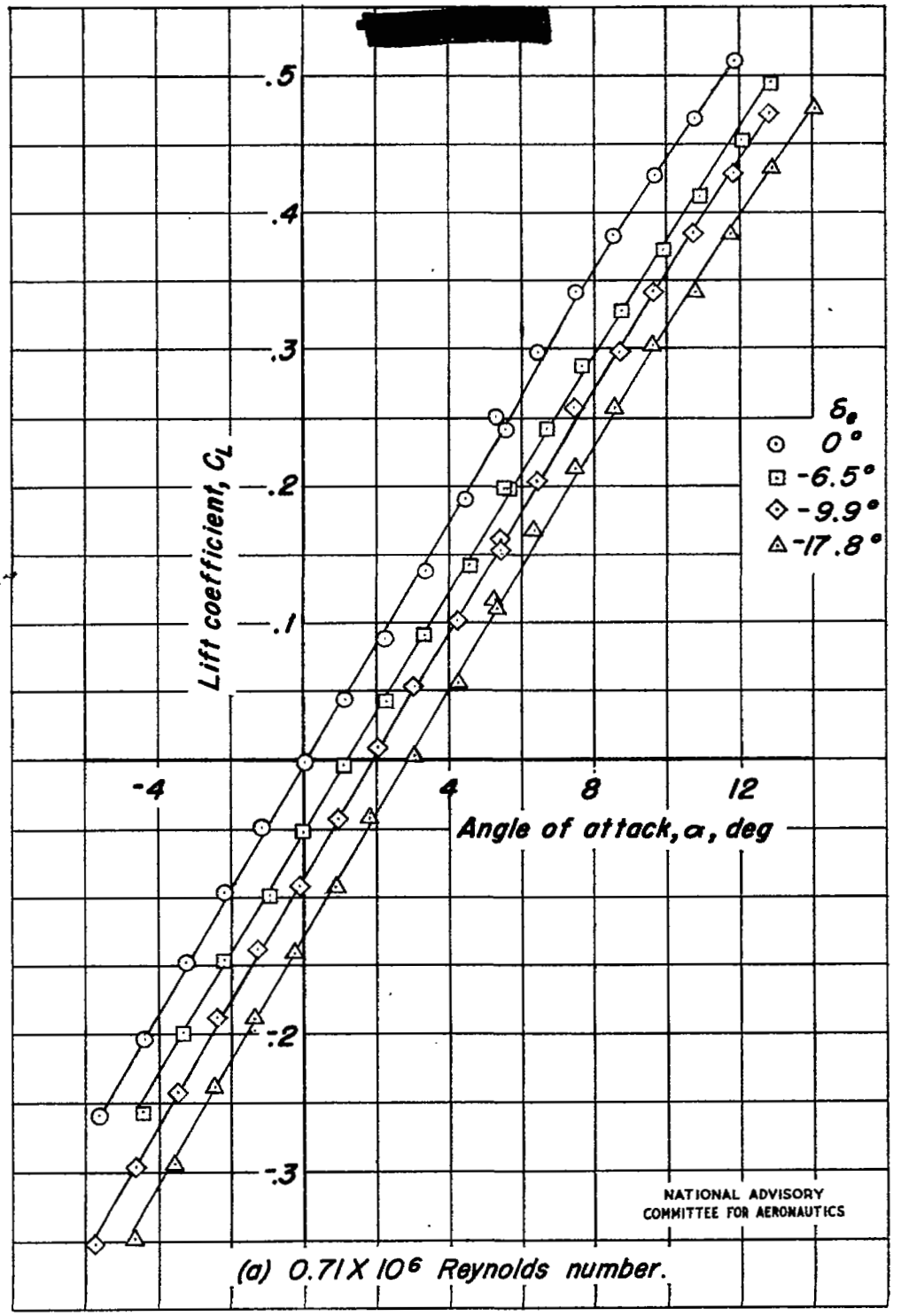

(a) 0.71×10^6 Reynolds number.

Figure 21.- Effect of elevator deflection on the variation of lift coefficient with angle of attack for configuration $B_s W_{60} V_1$.

[redacted]

[redacted]

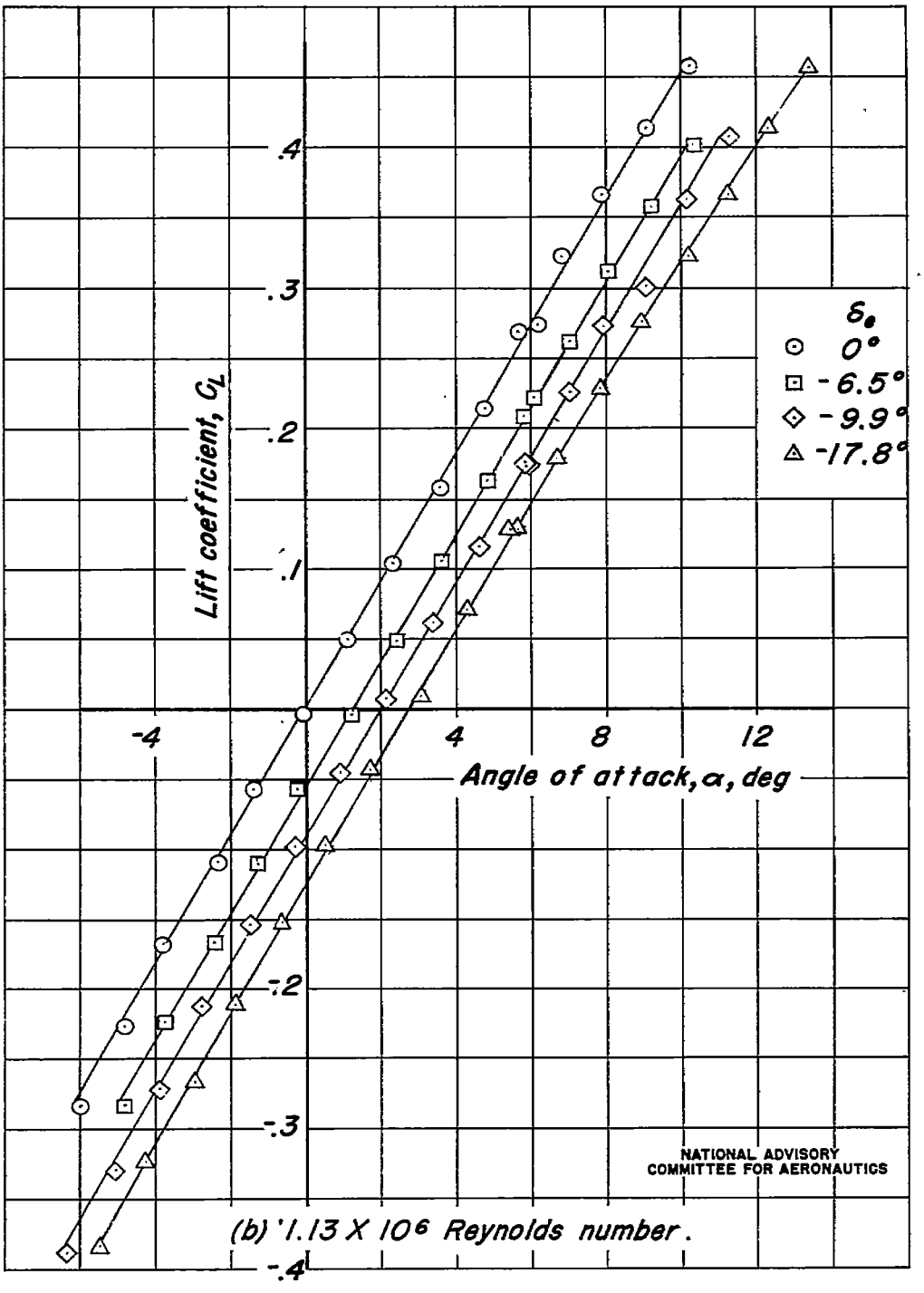

(b) 1.13 X 10^6 Reynolds number.

Figure 21.- Concluded.

[redacted]

[redacted]

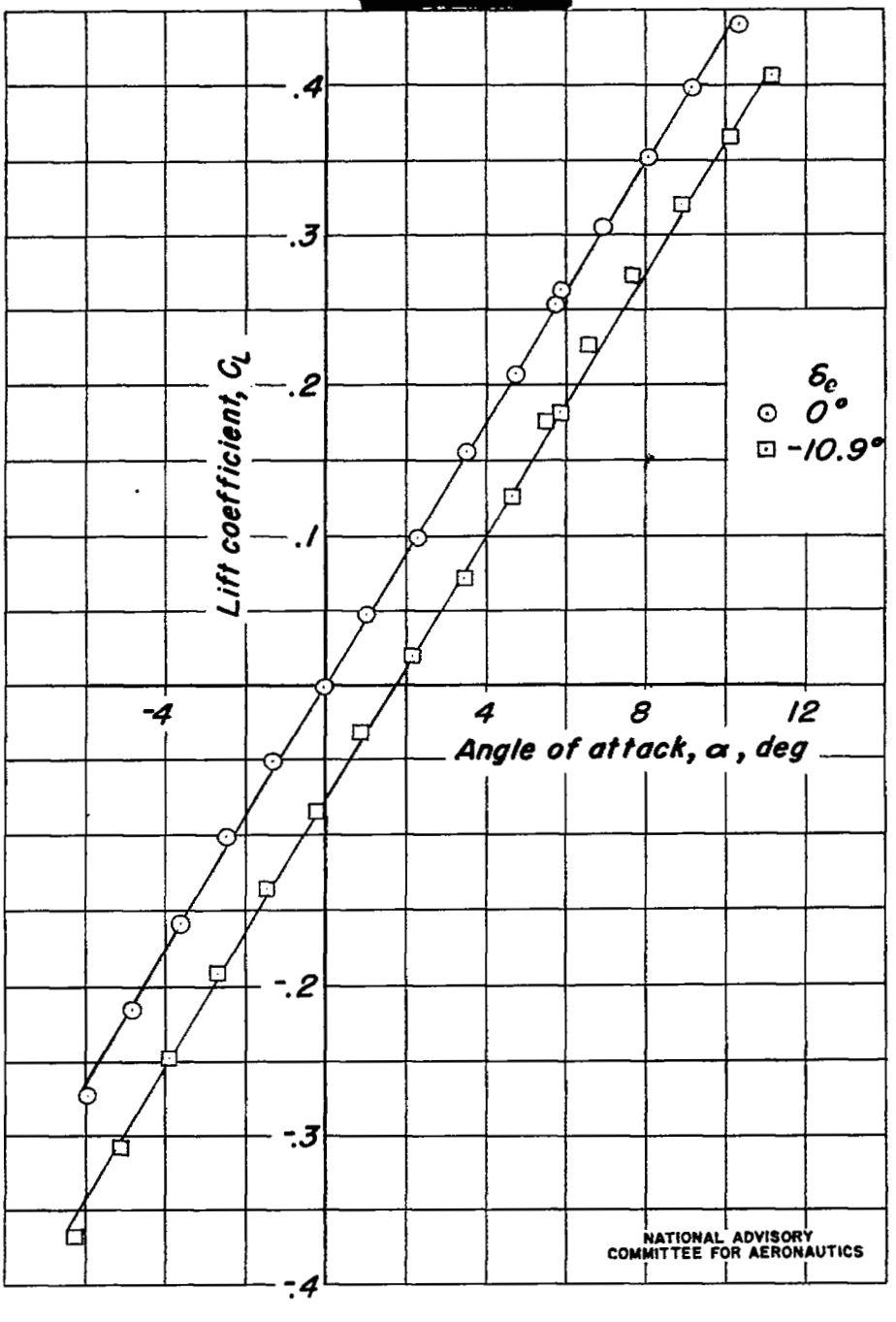

Figure 22. - Effect of elevator deflection on the variation of lift coefficient with angle of attack for configuration $B_S W_{60} V_2$ at 1.13×10^6 Reynolds number. [redacted]

[redacted]

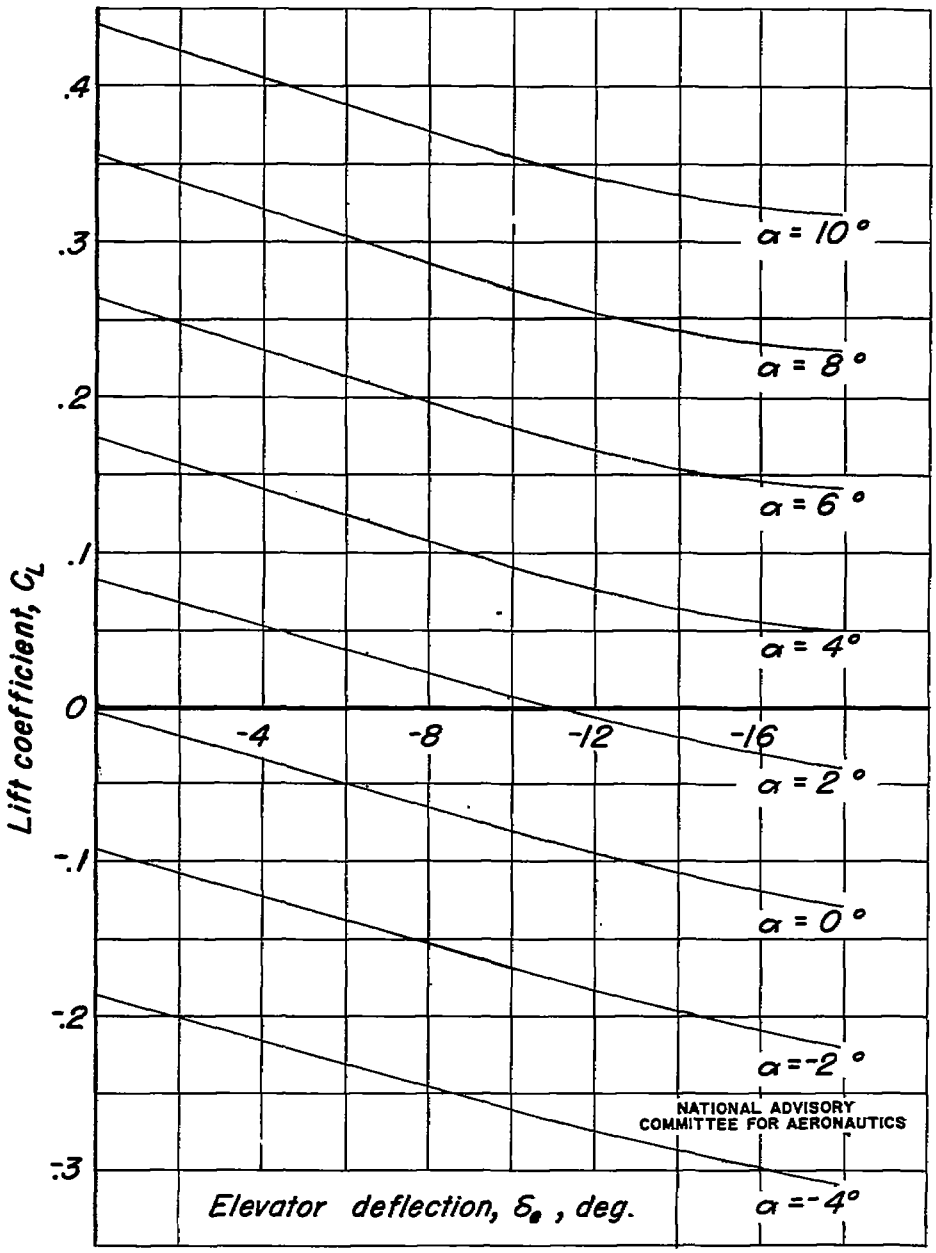

(a) 0.71×10^6 Reynolds number.

Figure 23. - Variation of lift coefficient with elevator deflection at several angles of attack for configuration $B_S W_{60} V_1$.

[redacted]

[redacted]

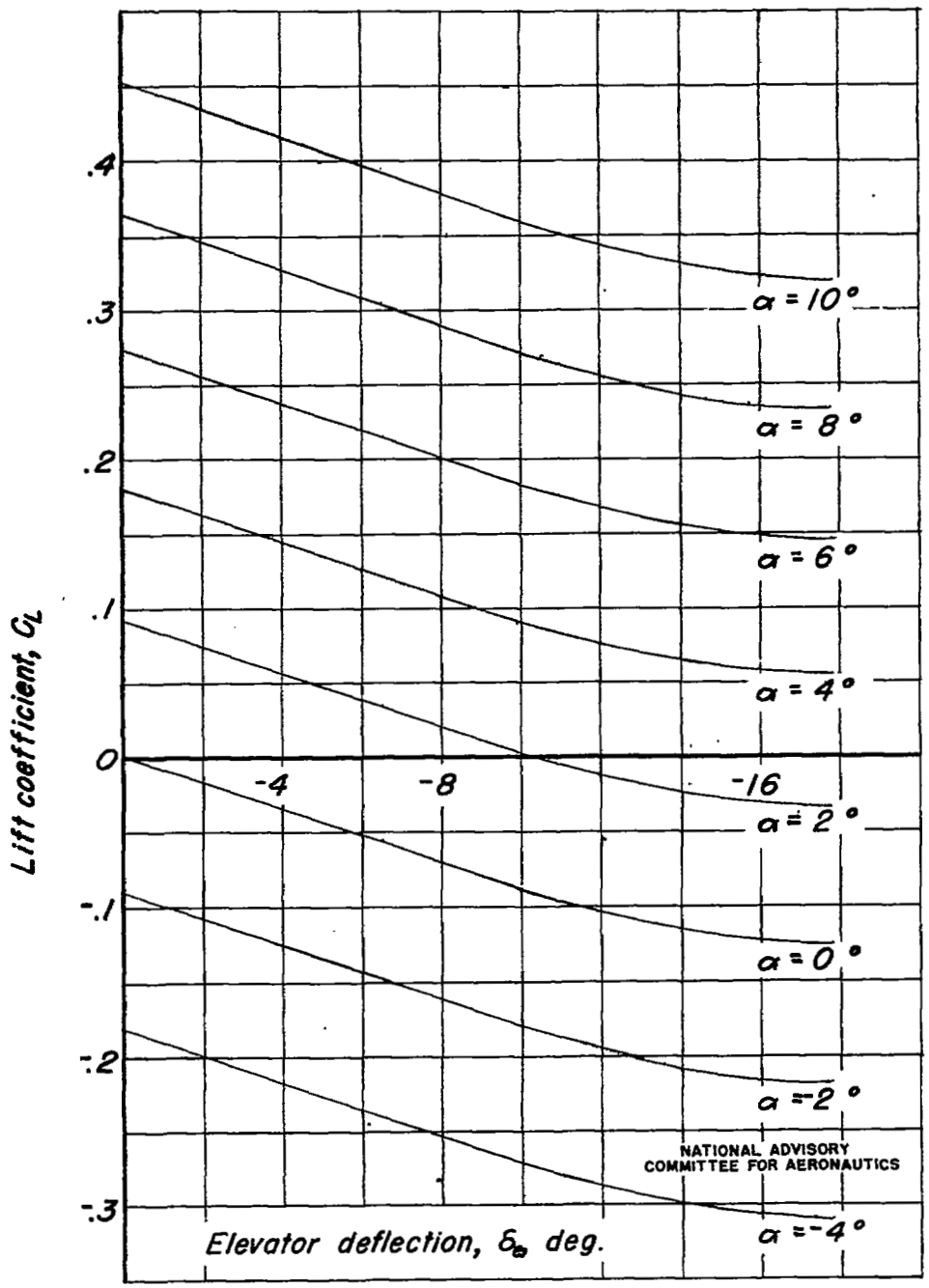

(b) 1.13 X 10^6 Reynolds number

Figure 23.- Concluded.

[redacted]

[redacted]

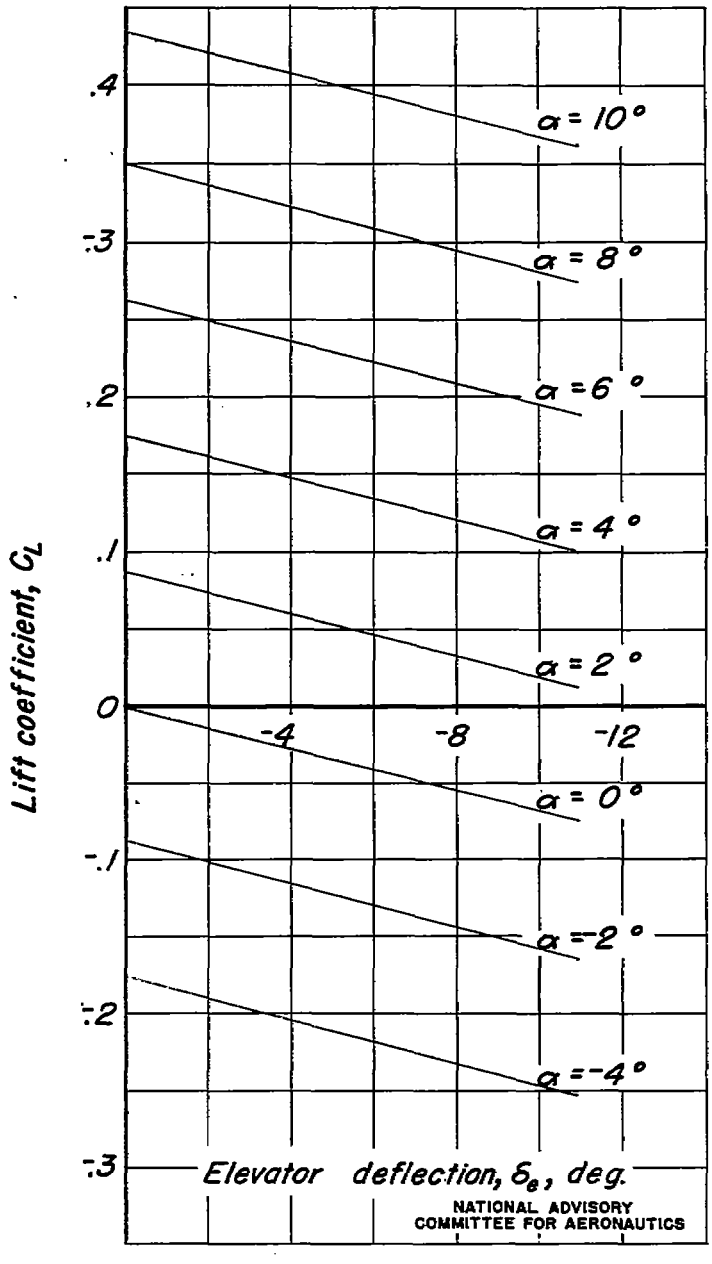

Figure 24.- Variation of lift coefficient with elevator deflection at several angles of attack for configuration $B_sW_{60}V_2$ at 1.13×10^6 Reynolds number.

[redacted]

[redacted]

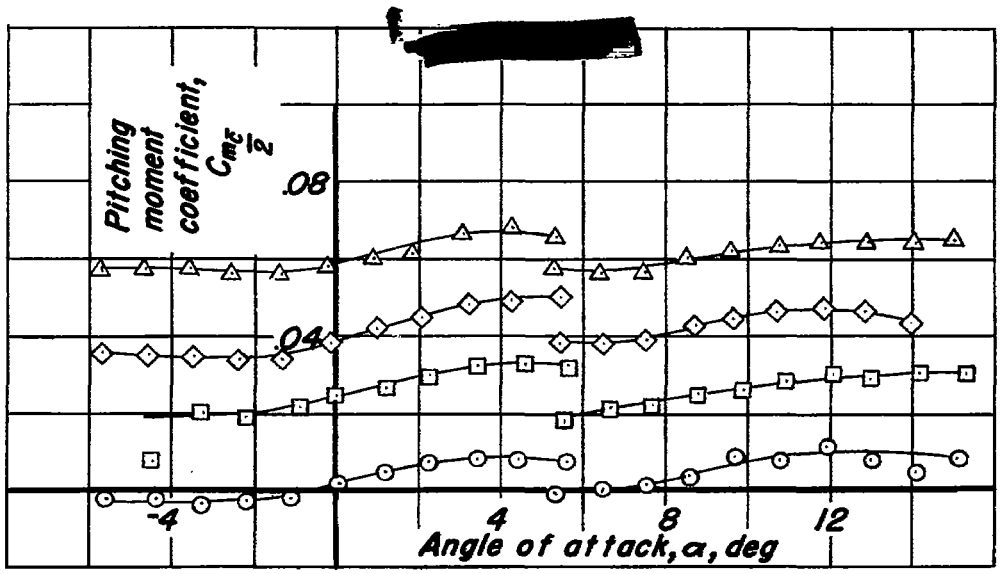

(a) 0.71×10^6 Reynolds number.

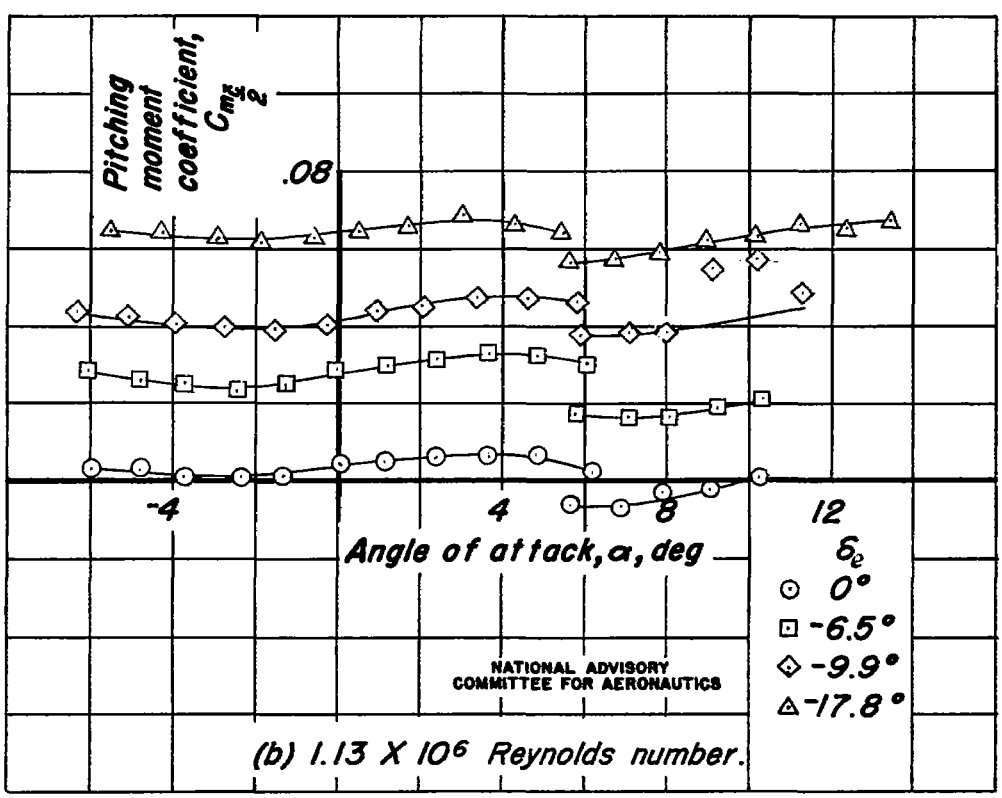

(b) 1.13×10^6 Reynolds number.

Figure 25.- Effect of elevator deflection on the variation of 50 percent m.a.c. pitching-moment coefficient with angle of attack for configuration $B_1W_{60}V_1$.

[redacted]

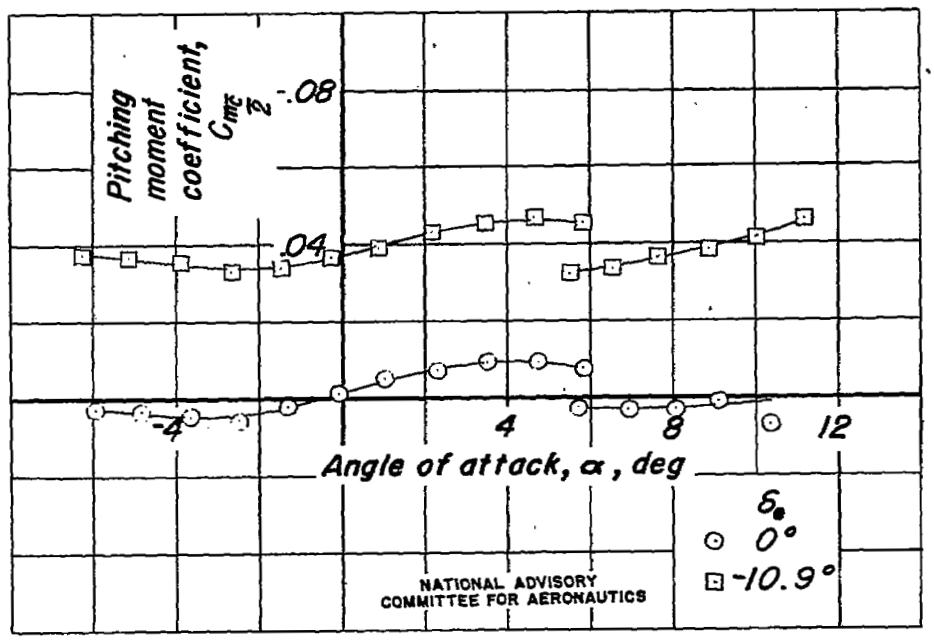

Figure 26.- Effect of elevator deflection on the variation of 50 percent m.a.c. pitching-moment coefficient with angle of attack for configuration $B_sW_{60}V_2$ at 1.13×10^6 Reynolds number.

[redacted]

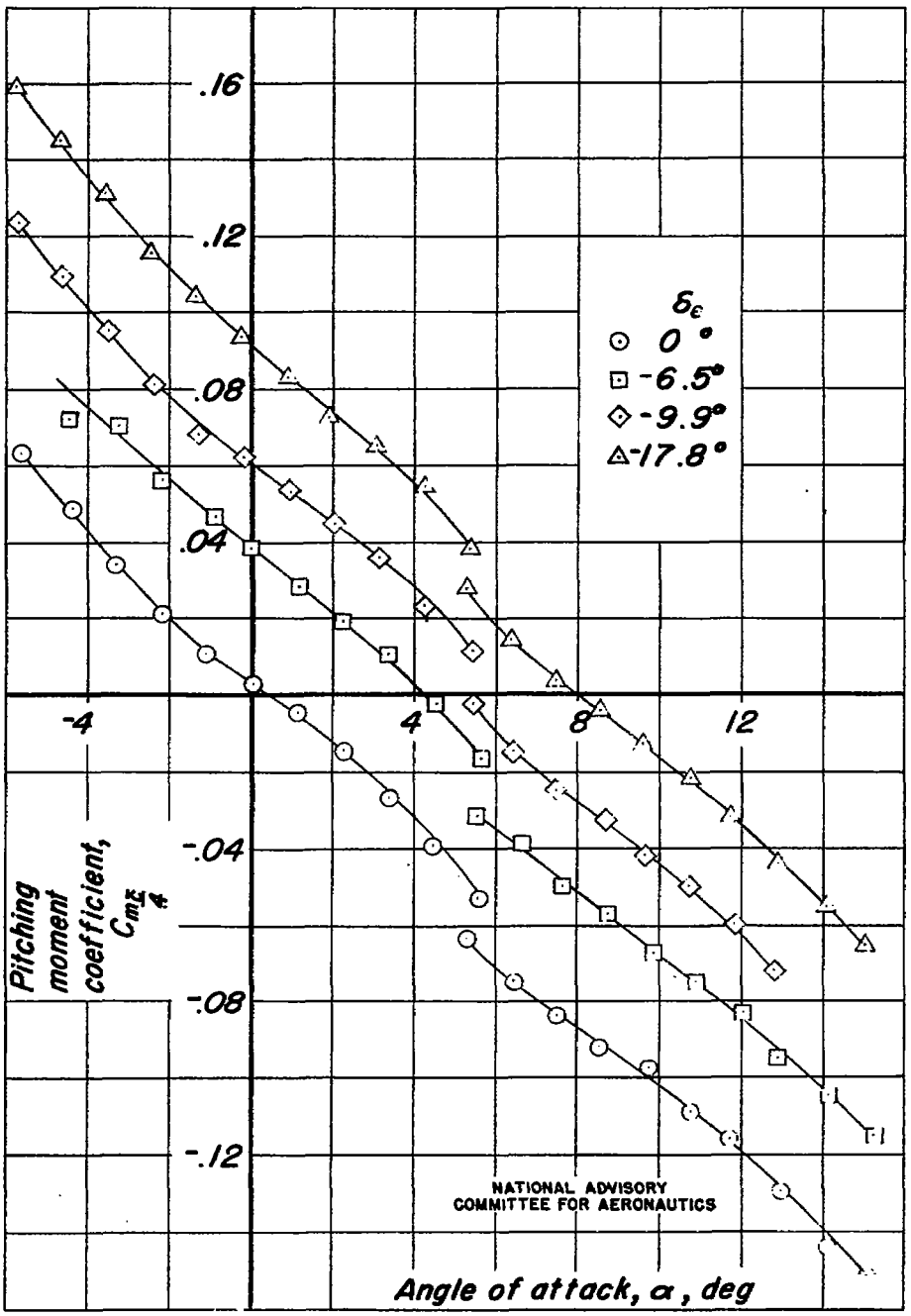

(a) 0.71 X 10⁶ Reynolds number.

Figure 27.- Effect of elevator deflection on the variation of 25 percent m.a.c. pitching-moment coefficient with angle of attack for [redacted] $B_sW_{60}V_1$.

[redacted]

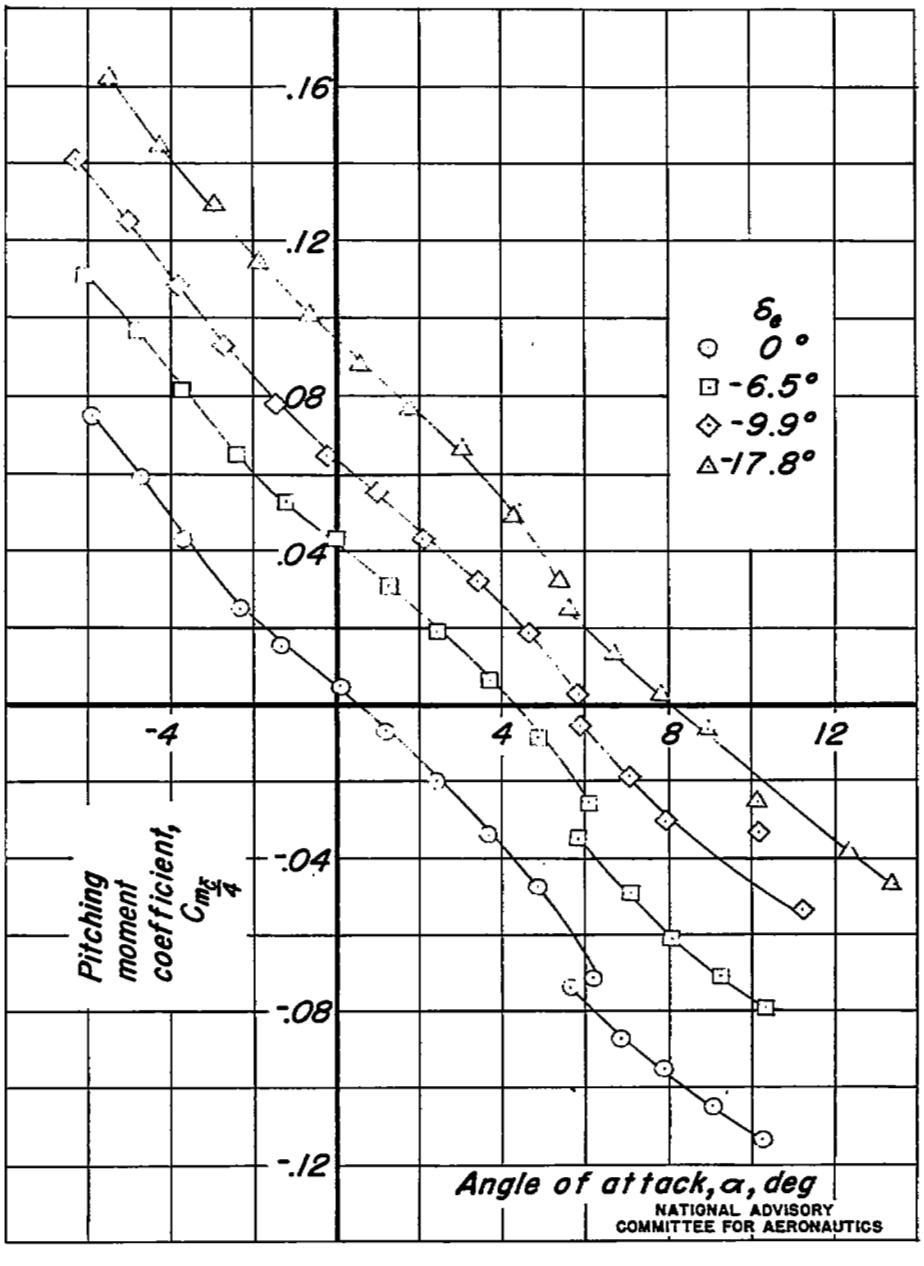

(b) 1.13 X 10^6 Reynolds number.

Figure 27.- Concluded.

[redacted]

[redacted]

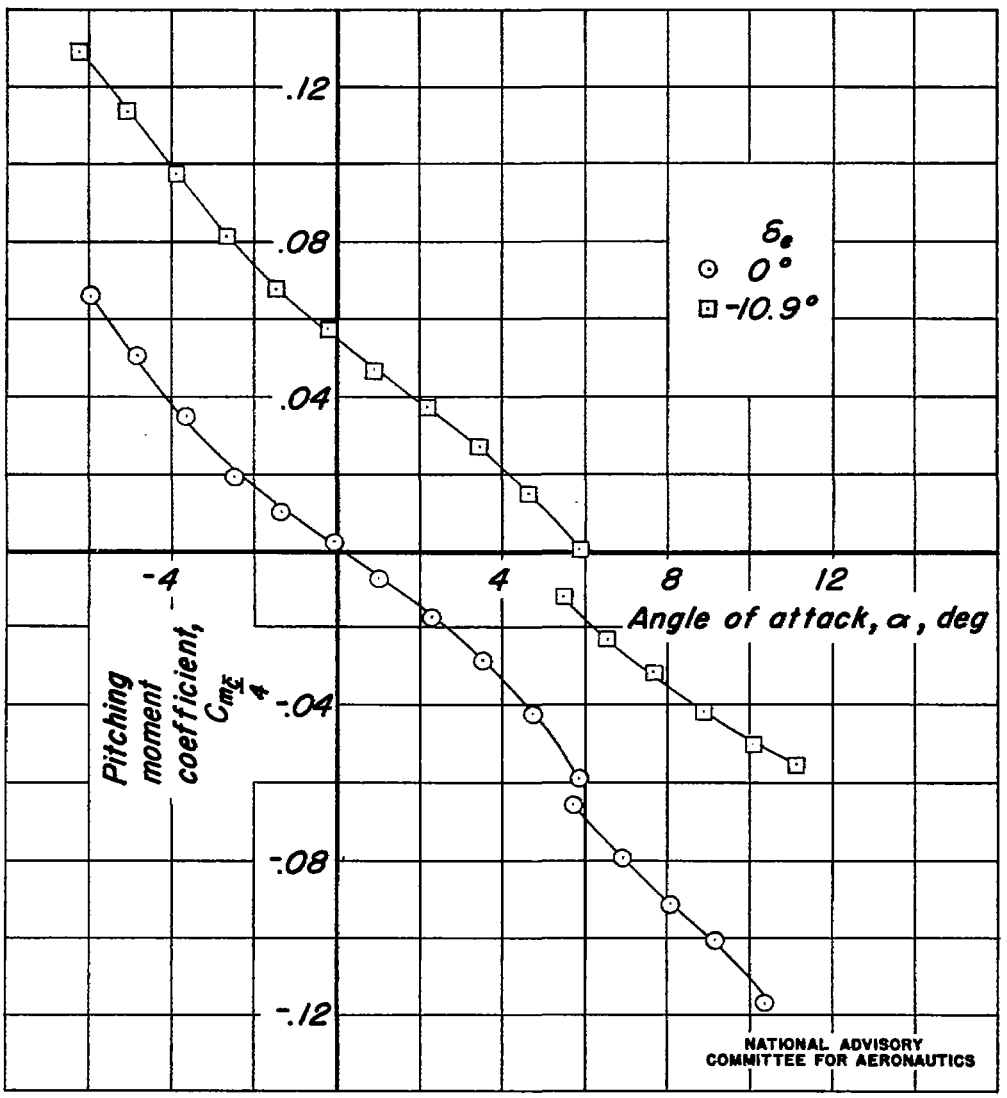

Figure 28.- Effect of elevator deflection on the variation of 25 percent m. a. c. pitching-moment coefficient with angle of attack for configuration B_S W_{60} V_1 at 1.13 X 10^6 Reynolds number.

[redacted]

[redacted]

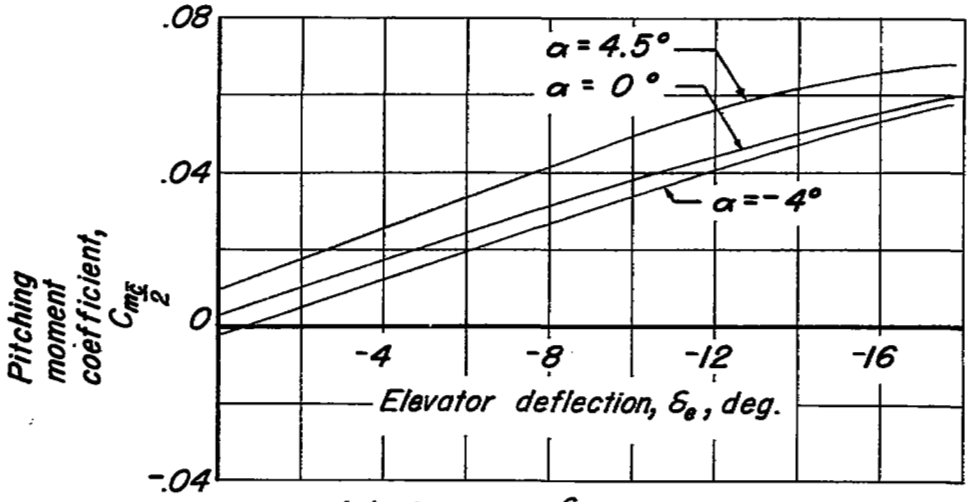

(a) 0.71 X 10^6 Reynolds number.

Note: Data for all other angles of attack fall between limits shown.

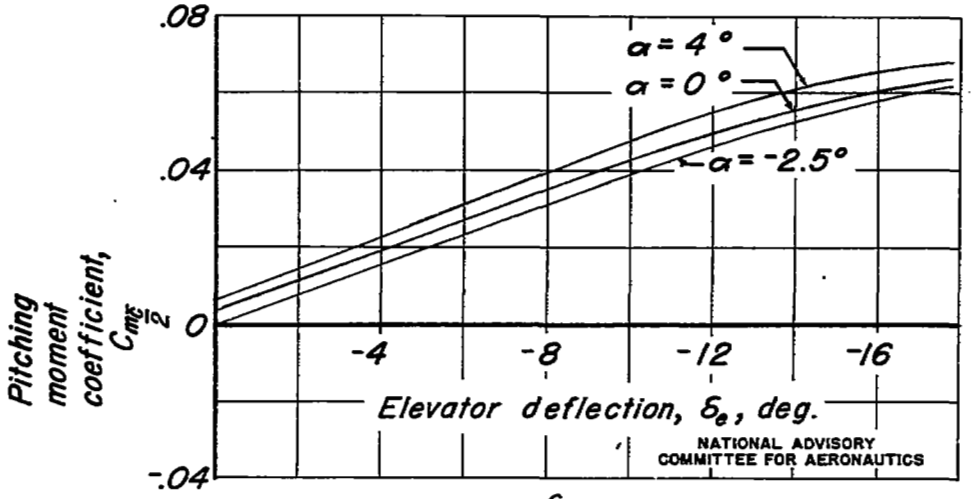

(b) 1.13 X 10^6 Reynolds number.

Figure 29.- Variation of 50 percent m. a. c. pitching-moment coefficient with elevator deflection at several angles of attack for configuration $B_S W_{60} V_1$.

[redacted]

[redacted]

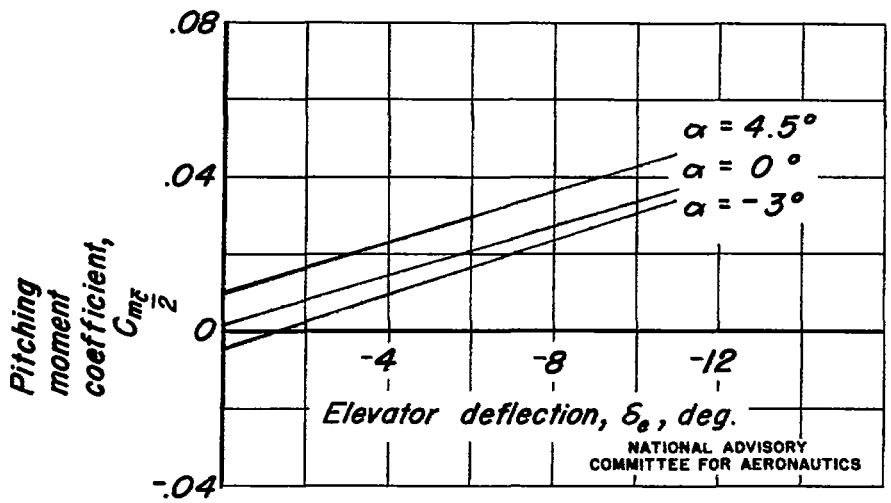

Note: Data for all other angles of attack fall between limits shown.

Figure 30. - Variation of 50 percent m. a. c. pitching-moment coefficient with elevator deflection at several angles of attack for configuration $B_S W_{60} V_2$ at 1.13×10^6 Reynolds number.

[redacted]

[redacted]

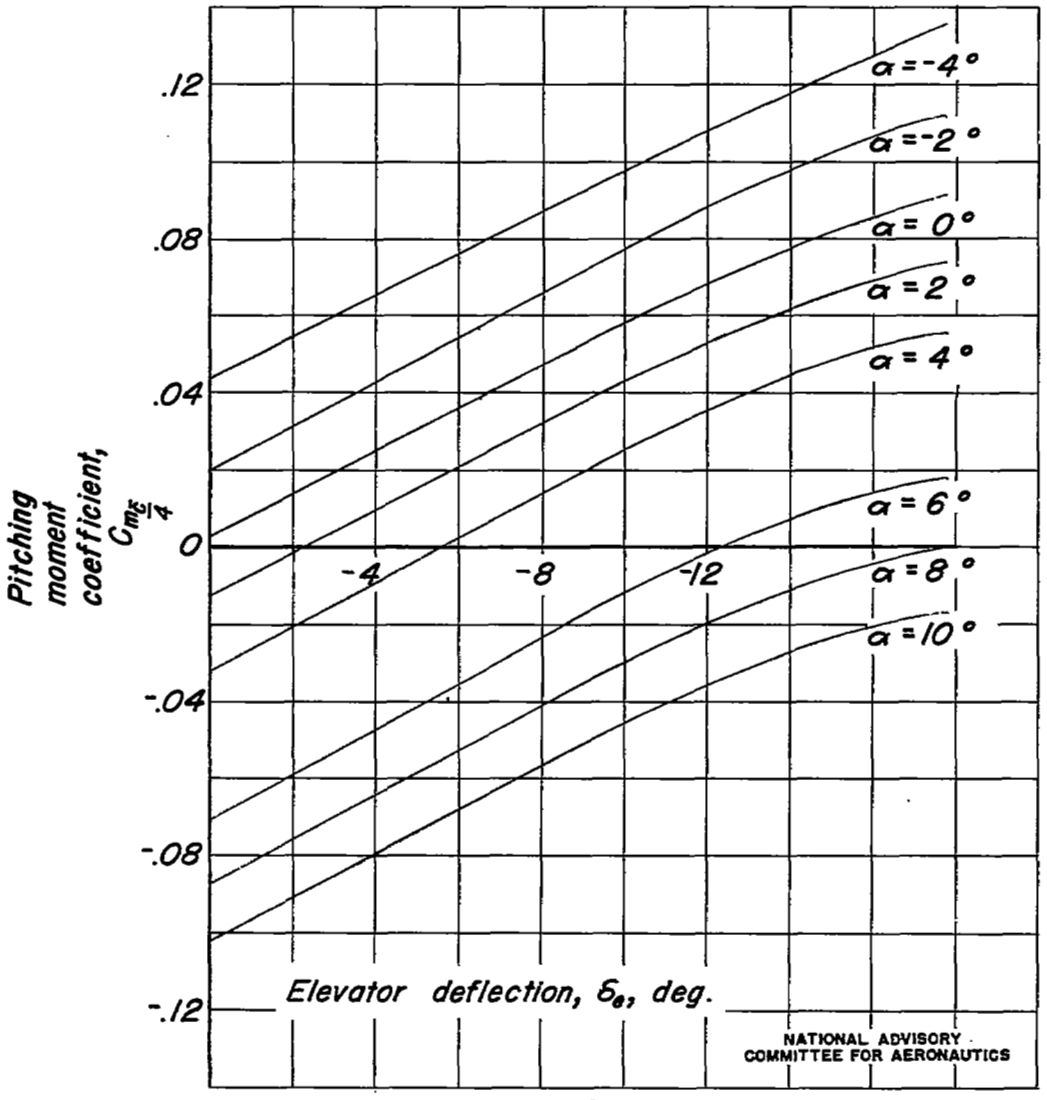

(a) 0.71×10^6 Reynolds number.

Figure 31. - Variation of 25 percent m. a. c. pitching-moment coefficient with elevator deflection at several angles of attack for configuration $B_S\ W_{60}\ V_1$.

[redacted]

[redacted]

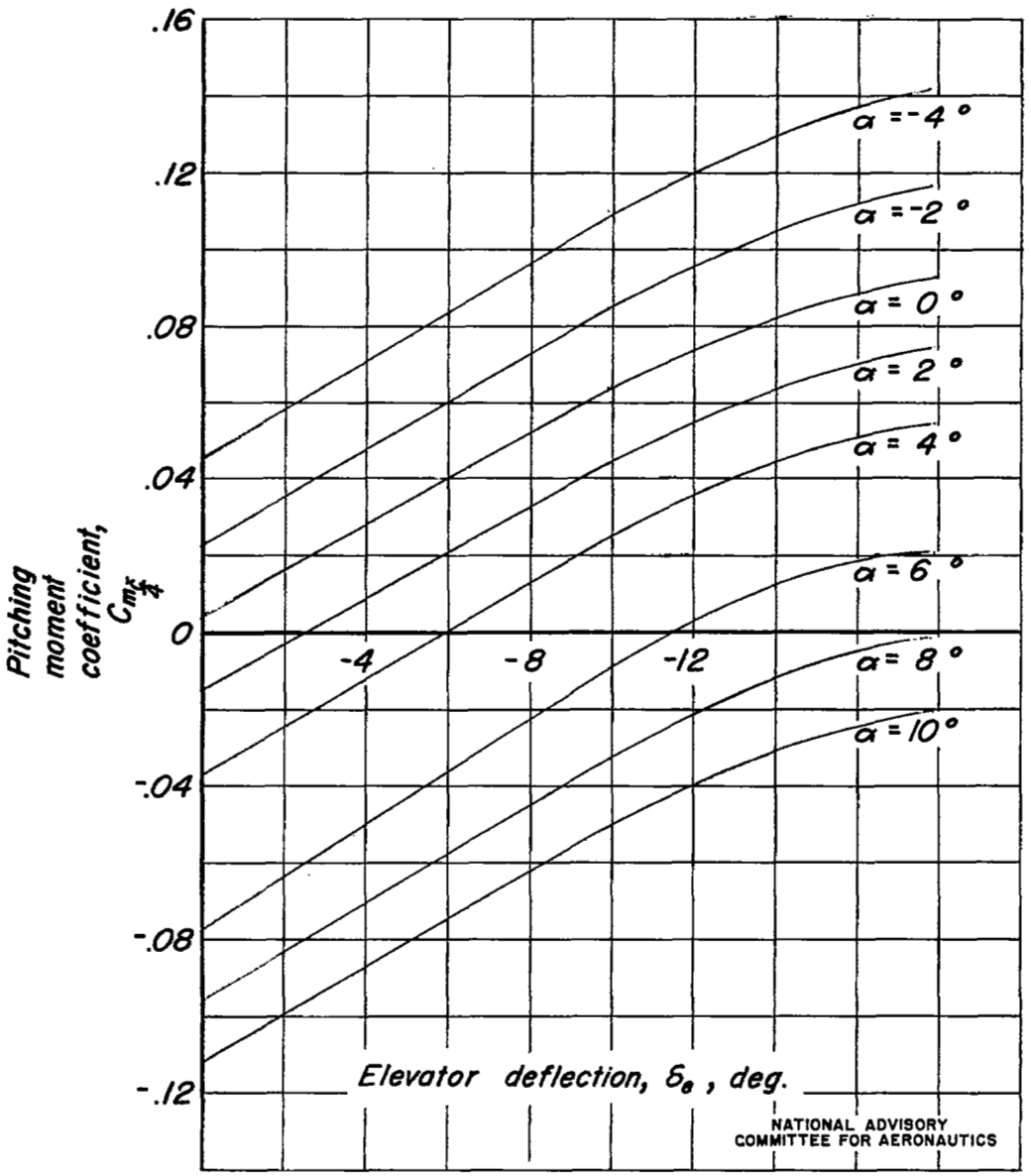

(b) 1.13×10^6 Reynolds number.

Figure 31. - Concluded.

[redacted]

[redacted]

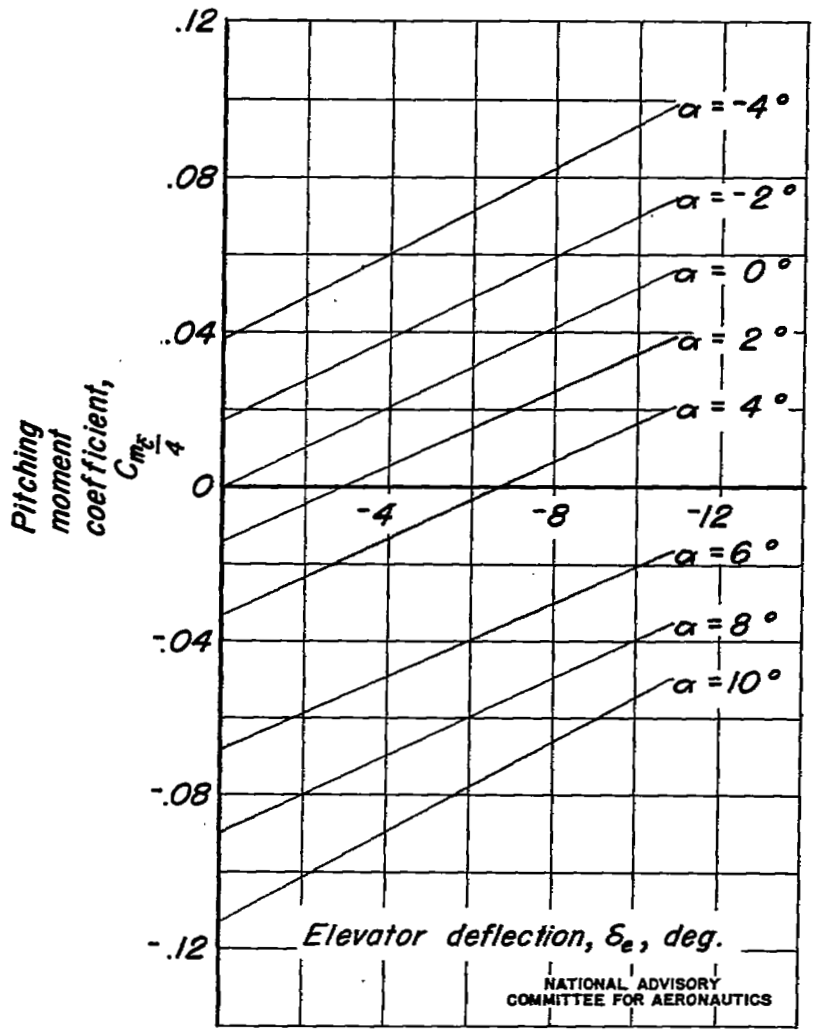

Figure 32.- Variation of 25 percent m.a.c. pitching-moment coefficient with elevator deflection at several angles of attack for configuration $B_s W_{60} V_2$ at 1.13×10^6 Reynolds number.

[redacted]

[redacted]

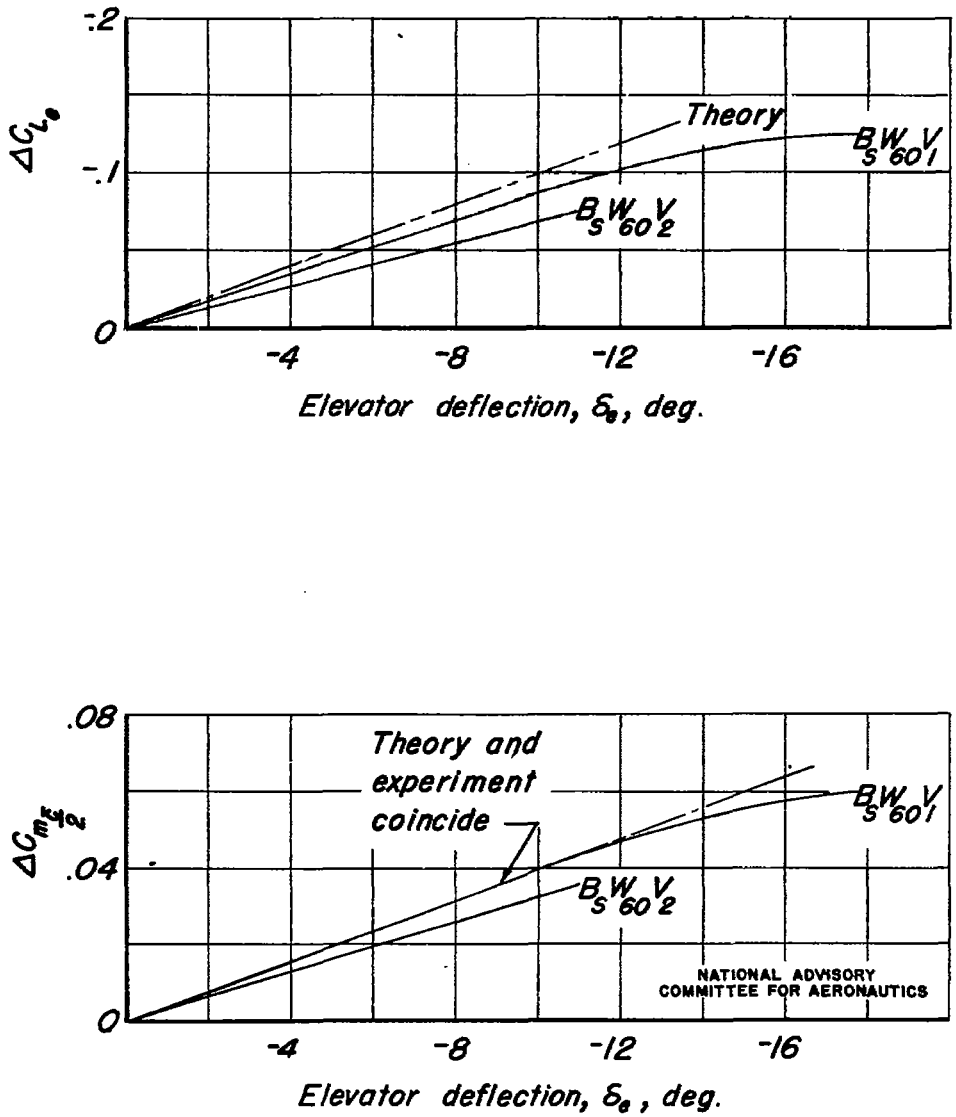

Figure 33.- Experimental and theoretical effects of elevator deflection on lift coefficient and 50 percent m.a.c. pitching-moment coefficient.

[redacted]

NASA Technical Library
3 1176 01434 4411